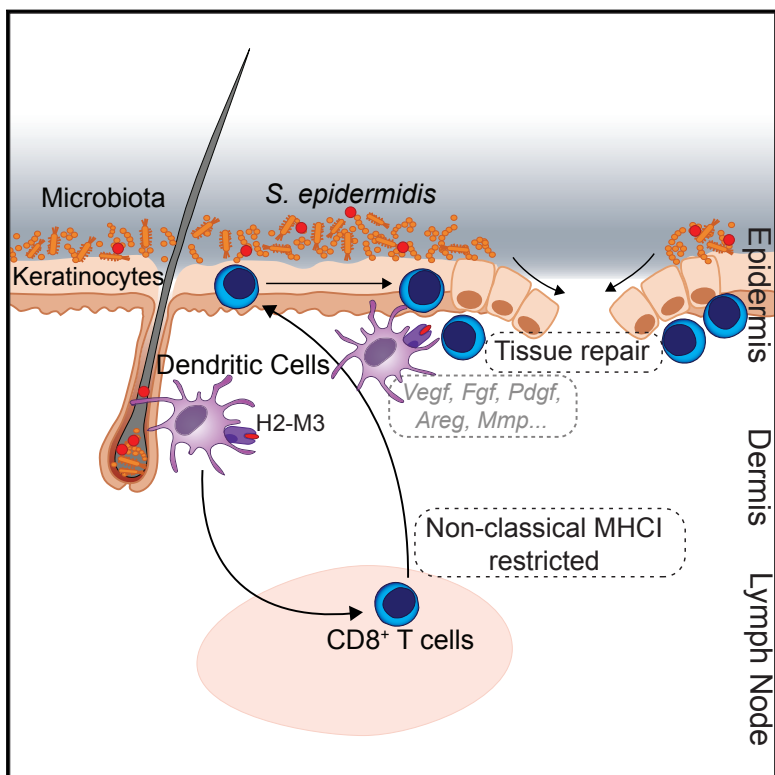


Non-classical Immunity Controls Microbiota Impact on Skin Immunity and Tissue Repair

Graphical Abstract



Authors

Jonathan L. Linehan, Oliver J. Harrison,
Seong-Ji Han, ..., Jason M. Brenchley,
John J. O'Shea, Yasmine Belkaid

Correspondence

ybelkaid@niaid.nih.gov

In Brief

Microbiota induce a form of adaptive immunity that couples antimicrobial function with tissue repair.

Highlights

- Non-classical MHC class I molecules promote homeostatic immunity to the microbiota
- Commensal-specific T cells express immunoregulatory and tissue repair signatures
- Commensal-specific T cells accelerate wound closure



Non-classical Immunity Controls Microbiota Impact on Skin Immunity and Tissue Repair

Jonathan L. Linehan,¹ Oliver J. Harrison,¹ Seong-Ji Han,¹ Allyson L. Byrd,^{1,2,3} Ivan Vujkovic-Cvijin,¹ Alejandro V. Villarino,⁴ Shirjo K. Sen,⁵ Jahangheer Shaik,⁶ Margery Smelkinson,⁷ Samira Tamoutounour,¹ Nicholas Collins,¹ Nicolas Bouladoux,^{1,8} Amiran Dzutsev,⁵ Stephan P. Rosshart,⁹ Jesse H. Arbuckle,¹⁰ Chyung-Ru Wang,¹¹ Thomas M. Kristie,¹⁰ Barbara Rehermann,⁹ Giorgio Trinchieri,⁵ Jason M. Brenchley,¹² John J. O'Shea,⁴ and Yasmine Belkaid^{1,13,*}

¹Mucosal Immunology Section, Laboratory of Parasitic Diseases, NIAID, NIH, Bethesda, MD 20892, USA

²Translational and Functional Genomics Branch, NHGRI, NIH, Bethesda, MD 20892, USA

³Department of Bioinformatics, Boston University, Boston, MA 02215, USA

⁴Molecular Immunology and Inflammation Branch, NIAMS, NIH, Bethesda, MD 20892, USA

⁵Cancer and Inflammation Program, NCI, NIH, Bethesda, MD 20892, USA

⁶Laboratory of Parasitic Diseases, NIAID, NIH, Bethesda, MD 20892, USA

⁷Biological Imaging, Research Technology Branch, NIAID, NIH, Bethesda, MD 20892, USA

⁸NIAID Microbiome Program, NIH, Bethesda, MD 20892, USA

⁹Immunology Section, Liver Diseases Branch, NIDDK, NIH, Bethesda, MD 20892, USA

¹⁰Molecular Genetics Section, NIAID, NIH, Bethesda, MD 20892, USA

¹¹Department of Microbiology and Immunology, Northwestern University, Chicago, IL 60611, USA

¹²Barrier Immunity Section, Laboratory of Parasitic Diseases, NIAID, NIH, Bethesda, MD 20892, USA

¹³Lead Contact

*Correspondence: ybelkaid@niaid.nih.gov

<https://doi.org/10.1016/j.cell.2017.12.033>

SUMMARY

Mammalian barrier surfaces are constitutively colonized by numerous microorganisms. We explored how the microbiota was sensed by the immune system and the defining properties of such responses. Here, we show that a skin commensal can induce T cell responses in a manner that is restricted to non-classical MHC class I molecules. These responses are uncoupled from inflammation and highly distinct from pathogen-induced cells. Commensal-specific T cells express a defined gene signature that is characterized by expression of effector genes together with immunoregulatory and tissue-repair signatures. As such, non-classical MHC-restricted commensal-specific immune responses not only promoted protection to pathogens, but also accelerated skin wound closure. Thus, the microbiota can induce a highly physiological and pleiotropic form of adaptive immunity that couples antimicrobial function with tissue repair. Our work also reveals that non-classical MHC class I molecules, an evolutionarily ancient arm of the immune system, can promote homeostatic immunity to the microbiota.

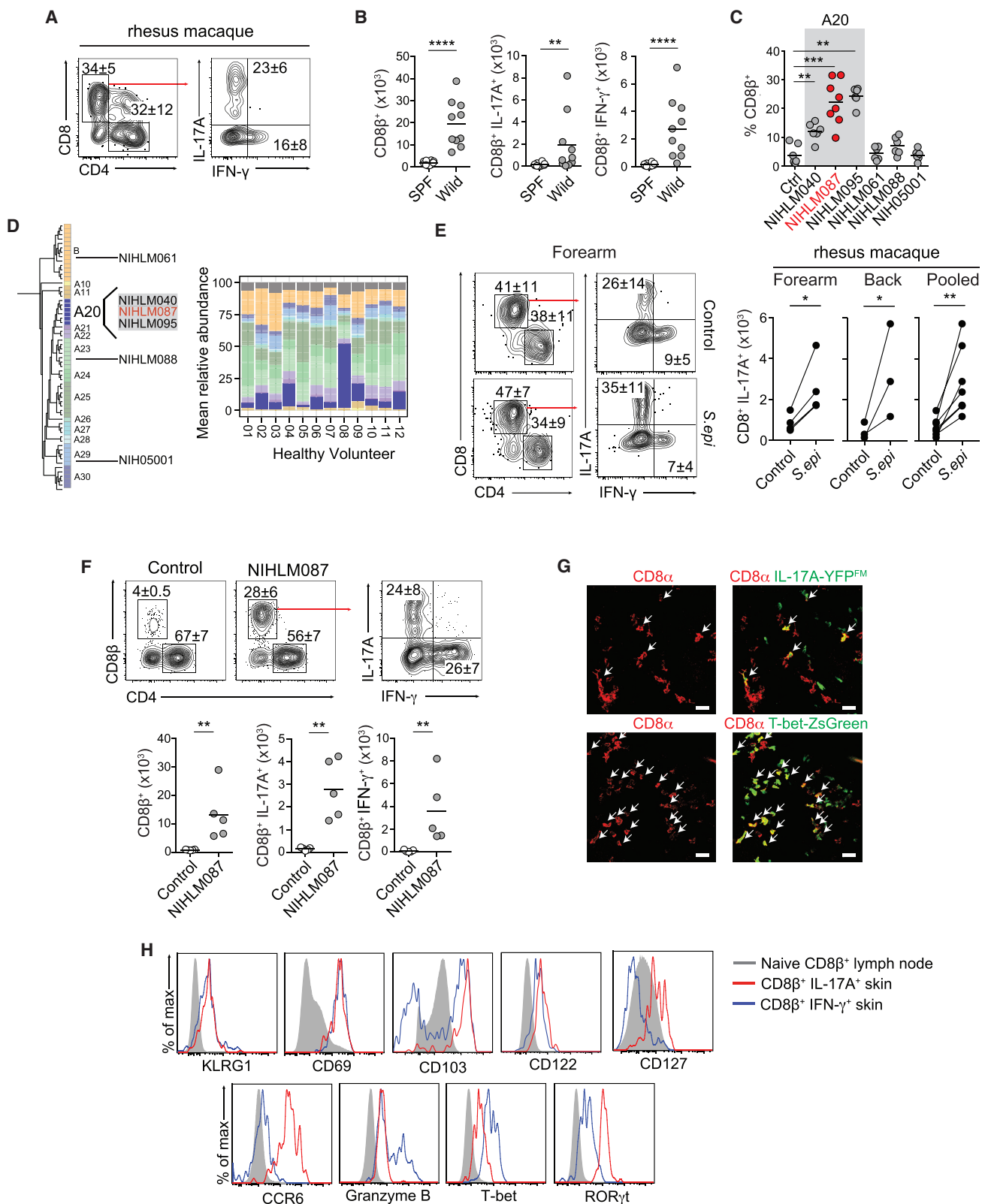
INTRODUCTION

The immune system acts as a formidable regulator of host homeostasis to sustain and restore tissue function in the context of microbial encounters and environmental challenges.

The development of defined arms of the immune system and, more particularly, those associated with adaptive immunity has coincided with the acquisition of a complex microbiota, suggesting that a large fraction of this machinery has evolved as a means to maintain symbiotic relationships with these highly diverse microbial communities (Belkaid and Hand, 2014).

Most of what we understand today about the function of the immune system has come from the exploration of inflammatory settings or responses to pathogenic microbes. However, the vast majority of immune system-microbial encounters are those resulting from the symbiotic relationship with the microbiota. The characteristics and properties of this class of immunity remain largely unknown. Far from being ignored by the immune system as originally perceived, microbes at all barrier surfaces are tonically educating tissues for antimicrobial functions and are actively recognized by both the innate and the adaptive immune systems (Belkaid and Hand, 2014; Honda and Littman, 2016; Pamer, 2016). In the gastrointestinal tract, host-microbe communications are mediated by immunoglobulin A (IgA), T helper 17 (Th17), and regulatory T (Treg) cell responses, a dialog that can be in part explained by the unique requirement of the gastrointestinal (GI) tract for absorption (Belkaid and Hand, 2014; Honda and Littman, 2016). However, it is now becoming clear that even at more stringent barrier sites, such as the skin, the immune system is poised to sense and to respond to the microbiota (Naik et al., 2015; Scharschmidt et al., 2015). These commensal-specific responses not only control microbiota containment but also promote antimicrobial defenses via their action on both innate and epithelial cells (Ivanov et al., 2009; Naik et al., 2015; Yang et al., 2014). However, despite the extraordinary number of potential





(legend on next page)

antigens expressed by the microbiota, only a handful of epitopes have been identified thus far (Cong et al., 2009; Yang et al., 2014), and the mechanisms underlying antigen presentation of microbiota-derived antigens remains poorly understood.

The skin is the body's most exposed environmental interface and acts as a first line of physical and immunological defense. This organ is also a complex and dynamic ecosystem inhabited by a multitude of microorganisms including bacteria, fungi, and viruses (Belkaid and Segre, 2014). Skin-specific microbiota control diverse aspects of tissue physiology, including innate and adaptive immunity to pathogens (Belkaid and Tamoutounour, 2016). Even in the context of an intact barrier, an encounter of the skin immune system with a commensal or mutualistic microbe can drive cognate, long-lasting immune responses that promote broad antimicrobial responses (Naik et al., 2015). One striking feature of commensal-specific immunity is its uncoupling from inflammation and the maintenance of tissue homeostasis at both the induction and the effector stages of the response (Naik et al., 2015). These observations raise several intriguing questions. Particularly, to what extent does adaptive immunity induced under these physiological settings obey conventional rules of adaptive immunity to pathogens, and what are the defining properties of such homeostatic immune responses? Here, we show that commensal-derived *N*-formyl methionine-containing (fMet) peptides can be presented by a member of an ancient and evolutionarily conserved arm of the immune system. These results provide direct evidence that non-classical major histocompatibility complex class I (MHC Ib) molecules can function to present commensal-derived antigens to T cells and are thereby direct mediators in the interaction between the host and its microbiota. This work also reveals an ancient form of immunity endowed with a pleiotropic arsenal of immune functions ranging from protective immunity to tissue repair.

RESULTS

Staphylococcus epidermidis Elicits Tc17 and Tc1 Cells to Skin

We previously demonstrated in mice that skin association with defined commensals that persist at low levels leads to the induction of CD8 $^+$ T cells in the absence of inflammation (Naik et al., 2015). The accumulation of CD8 $^+$ T cells able to express interleukin-17A (IL-17A) (Tc17) or interferon-gamma (IFN- γ) (cytotoxic T cell [Tc1]) is also a common feature of the skin tissue in non-human primates and humans under steady-state conditions (Naik et al., 2015) (Figures 1A and S1A). Further, wild-caught outbred mice that are exposed to physiological microbial partners (Beura et al., 2016) contained a significantly increased number of IL-17A and IFN- γ -producing CD8 $^+$ T cells in the skin compared to specific pathogen-free (SPF) C57BL/6 mice (Figure 1B). Skin accumulation of CD8 $^+$ T cells can also be reproduced in SPF mice colonized with defined skin commensals such as *S. epidermidis* (Naik et al., 2015). Taken together, these observations point toward the physiological relevance of skin-resident Tc17 and Tc1 and suggest homeostatic functionality.

Using a collection of fully sequenced *S. epidermidis* isolates from both healthy donors and patients with nosocomial infections (Conlan et al., 2012), we found that while several isolates tested promoted the accumulation of Th1 and Th17 within the skin (Figure S1B), the ability of *S. epidermidis* to induce CD8 $^+$ T cell responses was restricted to isolates belonging to a specific clade (A20) (Figures 1C and 1D). This clade is highly represented on human skin and is enriched in healthy adults compared to pediatric atopic dermatitis patients (Byrd et al., 2017) (Figure 1D). Topical association of NIHLM087 (from A20 clade) to the skin of non-human primates (*rhesus macaque*) also significantly increased the absolute number of Tc17 cells, but not CD4 $^+$ T cells, in all animals tested (Figures 1E and S1C). Thus, the ability

Figure 1. Tc17 Cells Are Enriched in the Skin of Non-human Primates and Mice

- (A) Frequencies of IL-17A $^+$ or IFN- γ $^+$ CD8 $^+$ T cells isolated from rhesus macaque. All cells were isolated from the glabella. Left plot is gated on live CD45 $^+$ CD3 $^+$ T cells.
 - (B) Numbers of total, IL-17A $^+$, or IFN- γ $^+$ CD8 $^+$ T cells in naive SPF or wild-caught mice. All cells were isolated from ear pinnae. Plots are gated on live CD45 $^+$ TCR β $^+$ CD8 $^+$ T cells. Each dot represents an individual mouse.
 - (C) Frequencies of CD8 $^+$ T cells in control mice or mice topically associated with the indicated *S. epidermidis* isolate. *S. epidermidis* isolate highlighted in red (NIHLM087) is the strain used for all remaining experiments unless otherwise specified. All cells were isolated from ear pinnae. Plots are gated on live CD45 $^+$ TCR β $^+$ CD8 $^+$ T cells. Each dot represents an individual mouse.
 - (D) Phylogenetic tree of *S. epidermidis* clades and relative abundance plot of *S. epidermidis* clades across healthy volunteers. Individual bacterial clades are differentiated by color.
 - (E) Frequencies and numbers of IL-17A $^+$ or IFN- γ $^+$ CD8 $^+$ T cells in unassociated (control) or 2 weeks post-*S. epidermidis* (NIHLM087) association (contralateral side) isolated from rhesus macaques. All cells were isolated from dorsal forearm or upper back. Left plot is gated on live CD45 $^+$ CD3 ϵ $^+$ T cells. Paired points denote the same animal.
 - (F) Frequencies and numbers of total, IL-17A $^+$, or IFN- γ $^+$ CD8 $^+$ T cells in naive SPF mice (control) or 2 weeks post-*S. epidermidis* (NIHLM087) association. All cells were isolated from ear pinnae. Left plots are gated on live CD45 $^+$ TCR β $^+$ T cells. Each dot in the graph represents an individual mouse.
 - (G) Representative confocal imaging volume projected along the z axis of epidermal skin from mice 14 days post-*S. epidermidis* (NIHLM087) association. Arrows show CD8 α $^+$ IL-17A-Cre $^+$, Rosa26-YFP $^+$ (IL-17A-YFP $^{\text{FM}}$ = fate map) (top), and CD8 α $^+$ T-bet-ZsGreen $^+$ (bottom) cells. Scale bars, 20 μm .
 - (H) Expression of KLRG1, CD69, CD103, CD122, CD127, CCR6, granzyme B, T-bet, or ROR γ t by CD8 $^+$ T cells in ear pinnae of mice 2 weeks post-*S. epidermidis* association. Plots are gated on live CD45 $^+$ TCR β $^+$ CD8 $^+$ T cells. Solid gray, CD44 $^{\text{low}}$ CD8 $^+$ T cells in skin-draining lymph nodes (SLNs). Blue line, IFN- γ $^+$ CD8 $^+$ T cells in ear pinnae. Red line, IL-17A $^+$ CD8 $^+$ T cells in ear pinnae.
- Cells were stimulated with phorbol myristate acetate (PMA) and ionomycin (A–C, E, and F). Student's t test was used to measure significance (B–C and F). **p < 0.005, ***p < 0.0005, and ****p < 0.0001. Paired Student's t test was used to measure significance. *p < 0.05, **p < 0.005 (E). In (A), (E), and (F), the numbers in flow cytometry plots correspond to the frequencies of gated populations \pm SD. Data are representative of 2–3 independent experiments. See also Figure S1.

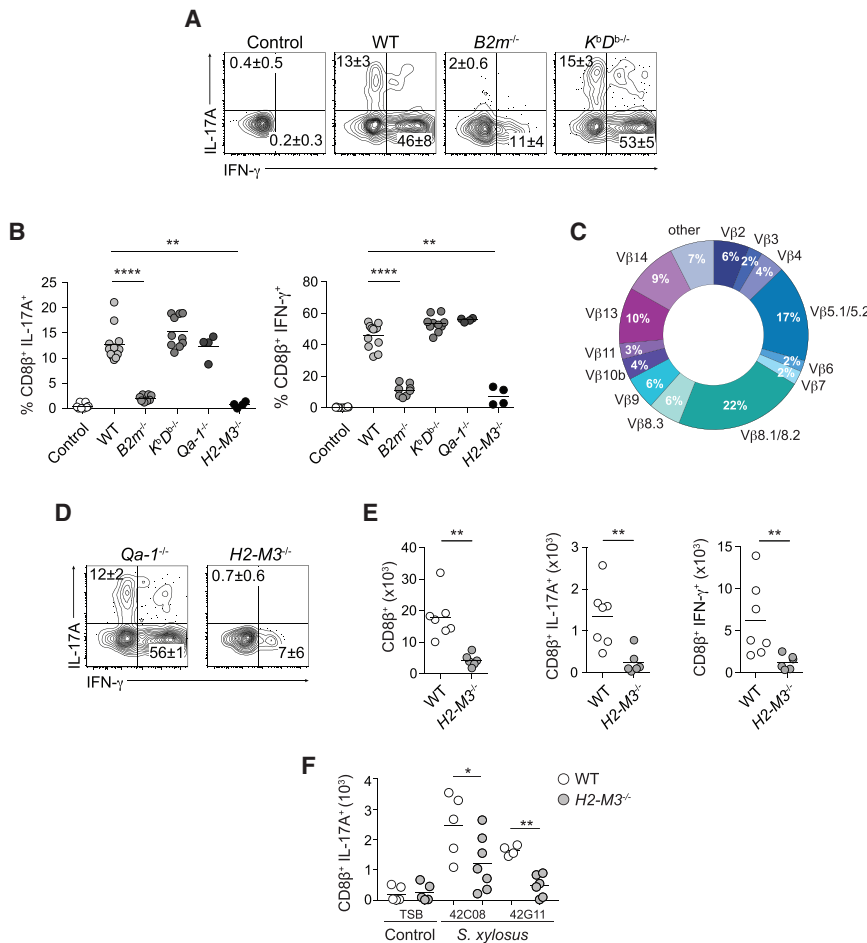


Figure 2. *S. epidermidis*-Specific CD8 $^+$ T Cells Are Restricted to the MHCb Molecule H2-M3

(A, B, and D) *In vitro* recall of *S. epidermidis*-induced CD8 $^+$ T cells from skin with heat-killed *S. epidermidis*-loaded splenic DCs. Representative flow cytometry plots (A and D) and dot plots (B) of frequencies of IL-17A $^+$ or IFN- γ $^+$ CD8 β $^+$ T cells after overnight culture. Splenic dendritic cells were enriched from wild-type (WT), $B2m^{-/-}$, $K^bD^{b/-}$, $Qa-1^{-/-}$, or $H2-M3^{-/-}$ mice. Control, unloaded WT splenic DCs. In (A) and (D), numbers in flow cytometry plots correspond to the frequency of gated populations \pm SD.

(C) Frequencies of V β chain usage among total CD8 β $^+$ T cells from skin.

(E) Numbers of total, IL-17A $^+$, or IFN- γ $^+$ CD8 β $^+$ T cells in *S. epidermidis*-associated WT or $H2-M3^{-/-}$ mice. Cells were stimulated with PMA and ionomycin.

(F) Numbers of IL-17A $^+$ CD8 β $^+$ T cells in WT or $H2-M3^{-/-}$ mice topically associated with tryptic soy broth (TSB) (control) or the indicated *S. xylosus* isolate. Each dot represents an individual mouse. All cells were isolated from ear pinnae of *S. epidermidis*- or *S. xylosus*-associated mice 2 weeks after application. Plots are gated on live CD45 $^+$ TCR β $^+$ CD8 β $^+$ T cells. (B, E, and F) Each dot represents an individual mouse. Student's t test was used to measure significance. *p < 0.05, **p < 0.005, and ***p < 0.0005. Data are representative of 2–4 independent experiments. See also Figure S2.

of *S. epidermidis* to promote skin CD8 $^+$ T cell responses is conserved in non-human primates.

In mice, Tc17 and Tc1 cells induced by NIHLM087 association (Figures 1F and 1G) shared phenotypic features with previously described pathogen-induced skin-resident memory CD8 $^+$ T cells. Notably, both subsets expressed high levels of CD69 and CD103 and low levels of killer cell lectin-like receptor G1 (KLRG1) and the IL-2R β subunit (CD122) (Figure 1H). Tc17 selectively expressed CCR6, ROR γ t, and the IL-7R α subunit (CD127), a phenotype that distinguishes them from both commensal-induced Tc1 (expressing T-bet, bimodal CD103, and granzyme B) and previously described skin T_{RM} (Schenkel and Masopust, 2014) (Figure 1H).

S. epidermidis-Specific CD8 $^+$ T Cells Are Restricted to MHCb

The homeostatic induction of CD8 $^+$ T cells in response to a non-invasive microbe led us to explore the possibility that unconventional mechanisms of antigen presentation may contribute to the initiation and/or maintenance of these responses. The *S. epidermidis*-specific CD8 $^+$ T cell response is β_2 -microglobulin (B2m)-dependent (Naik et al., 2015) (Figures 2A and 2B). The adaptor molecule B2m binds not only MHC α molecules but

also to numerous MHC β molecules (Rodgers and Cook, 2005). CD8 $^+$ T cells from previously associated wild-type (WT) mice were purified from the skin by cell sorting and incubated with $K^bD^{b/-}$ dendritic cells (DCs) loaded with heat-killed *S. epidermidis*. Both alleles of MHC α are deleted in $K^bD^{b/-}$ DCs (Vugmeyster et al., 1998). Bacteria loaded $K^bD^{b/-}$ DCs recalled IL-17A and IFN- γ production in a manner comparable to WT DCs, indicating that *S. epidermidis*-induced CD8 $^+$ T cells were restricted to an MHC β molecule (Figures 2A and 2B). Additionally, *S. epidermidis* loaded DCs isolated from several mouse strains (bearing non-complementary haplotypes) could recall CD8 $^+$ T cells similarly to DCs from C57BL/6 mice, formally demonstrating that CD8 $^+$ T cells isolated from the skin of *S. epidermidis* associated mice are restricted to a non-polymorphic B2m-dependent MHC β molecule (Figure S2A).

CD8 $^+$ T cell recall responses using *S. epidermidis*-conditioned media were equivalent to those obtained when DCs were loaded with heat-killed bacteria, supporting the idea that the antigen(s) sensed by the immune system was secreted (Figure S2B). Pre-incubation of the antigen preparation with the broad-spectrum serine protease proteinase K (Pro.K) prior to DC loading abolished the response (Figure S2B). In addition, $Tap1^{-/-}$ DCs phenocopied WT DCs in our recall assay, consistent with studies

showing that Tap1 is not necessary for peptide loading of some MHC Ib molecules (Rodgers and Cook, 2005) (Figure S2C). Together, these results indicate that the *S. epidermidis*-derived antigen(s) recognized by CD8 $^+$ T cells comes from secreted proteins, most likely peptides, processed and presented in a Tap1-independent manner.

CD8 $^+$ T cells induced by topical association with *S. epidermidis* utilized a diverse T cell receptor (TCR) V β usage pattern (Figure 2C). Among MHC Ib molecules, Qa-1 and H2-M3 are known to bind to TCRs with diverse V β chains (Lindahl et al., 1997). Although these molecules are considered “middle-aged” compared to other MHC Ib types, they emerged early in mammalian evolution (>65 million years ago), prior to the radiation of placental taxa (Doyle et al., 2003). Qa-1 and H2-M3 MHC Ib each bind a limited repertoire of both self and microbe-derived peptides; Qa-1 is specific for MHC I leader peptides and viral peptides and H2-M3 is specific for mitochondrial and bacterial peptides (Godfrey et al., 2015; Lindahl et al., 1997). *In vitro* recall of WT CD8 $^+$ T cells with *S. epidermidis*-loaded Qa-1 $^{+/-}$ DCs phenocopied the cytokine response elicited by WT loaded DCs (Figures 2B and 2D). However, IL-17A production by CD8 $^+$ T cells exposed to *S. epidermidis*-loaded H2-M3 $^{+/-}$ DCs was abrogated and the IFN- γ response was severely reduced compared to *S. epidermidis*-loaded WT DCs (Figures 2B and 2D). To assess the relevance of this pathway *in vivo*, we associated H2-M3 $^{+/-}$ and WT mice with *S. epidermidis*. Accumulation of both Tc17 and Tc1 was dramatically impaired in H2-M3 $^{+/-}$ compared to WT-associated mice (Figure 2E). Association of mice with isolates of a common murine skin commensal *Staphylococcus xylosus* also promoted CD8 $^+$ T cell accumulation in an H2-M3-dependent manner (Figure 2F). These results indicate that H2-M3 was required for the induction and/or function of CD8 $^+$ T cell responses to *S. epidermidis* and potentially to other dominant skin microbes.

***S. epidermidis*-Specific CD8 $^+$ T Cells Respond to *S. epidermidis*-Derived N-Formyl Methionine Peptides**

Next, we sought to identify the relevant bacterially derived H2-M3-bound antigenic ligands. H2-M3 binds peptides that contain an N-formyl methionine (fMet), which is required to initiate protein translation in bacteria and mitochondria (Lindahl et al., 1997). We interrogated the *S. epidermidis* genome for fMet peptides able to bind H2-M3, using a previously described algorithm that identifies peptides likely to bind H2-M3 based on a known sequence motif (Chun et al., 2001). Analysis of the *S. epidermidis* genome revealed 30 fMet peptides bearing this motif (Figure S3A). Two fMet peptides (f-MIIINA and f-MFLVN) could drive both IL-17A and IFN- γ production *in vitro* by *S. epidermidis*-elicited CD8 $^+$ T cells (Figures 3A and S3B).

To track *S. epidermidis*-specific CD8 $^+$ T cell responses *in vivo*, we generated an fMet peptide:H2-M3 tetramer reagent using f-MIIINA, the fMet peptide that triggered the strongest cytokine response during *in vitro* recall of *S. epidermidis*-specific CD8 $^+$ T cells (Figures 3A and S3B). In naive mice, no tetramer-positive cells were detected within the skin compartment. However, 7 days post-association with *S. epidermidis*, f-MIIINA:H2-M3 $^+$ CD8 $^+$ cells began to accumulate in this tissue (Figures 3B and 3C). Accumulation within peripheral tissues was restricted

to the skin and not detectable at other barrier sites such as the gastrointestinal tract (data not shown). From this time point and onward, ~5%–10% of total CD8 $^+$ T cells within the skin were f-MIIINA:H2-M3-specific, indicating that the response against this specific peptide was dominant and sustained for at least 1 month post-microbial colonization (Figures 3B and 3C).

Next, we assessed how systemic the response could be post-skin association by using a previously described method of tetramer staining followed by magnetic bead enrichment to identify all f-MIIINA:H2-M3-specific cells in skin-draining lymph nodes (SLNs) and spleen (Moon et al., 2007). We confirmed enrichment efficiency (Figure S3D) and that the tetramer bound MHC I -restricted CD8 $^+$ T cells, but not MHC II -restricted CD4 $^+$ T cells (Figure S3C). As an additional control for specificity, we stained the pooled secondary lymphoid organs (SLO) of naive mice with two f-MIIINA:H2-M3 tetramers each containing either phycoerythrin or allophycocyanin fluorochromes (Obar et al., 2008). Approximately 80% of tetramer binding cells bound to both tetramers, indicating this reagent stains f-MIIINA:H2-M3-specific cells with a high degree of specificity (Figure S3E). Next, we enumerated f-MIIINA:H2-M3-specific T cells within SLNs and spleen and detected an expanded population at day 5 post-association, a time point that preceded skin accumulation (Figure 3C). f-MIIINA:H2-M3-specific cell activation was first detectable at day 2 after *S. epidermidis* skin association in the SLNs (but not in the spleen) as evidenced by upregulation of CD69 (Figure S3F). These data support the idea that activation and expansion of H2-M3-restricted T cells first occurs in lymphoid structures, similar to conventional T cell responses. Further, these results reveal that response to a skin commensal is not restricted to the SLNs and can be more systemic than previously appreciated.

In naive mice, following tetramer staining and magnetic bead enrichment, we identified ~2500 f-MIIINA:H2-M3-specific cells in the pooled SLO (Figures 3C and 3D). Of note, the number of f-MIIINA:H2-M3-specific CD8 $^+$ cells in naive mice is high compared to the average number of naive CD8 $^+$ T cell precursors specific to foreign antigens presented by conventional MHC Ia pathways (~200 cells) (Obar et al., 2008). About half of the f-MIIINA:H2-M3-specific cells in pooled SLO were CD44 $^{\text{hi}}$, supporting the idea that these T cell receptors may have previously responded to other peptide:MHC I complexes. To test the possibility that *S. epidermidis* f-MIIINA:H2-M3-specific cells in naive SPF mice may be cross-reactive with pre-existing members of the microbiota, we assessed the frequency and phenotype of f-MIIINA:H2-M3-specific T cells in mice raised in the absence of live microbes (gnotobiotic). Surprisingly, the frequency of CD44 $^{\text{hi}}$ f-MIIINA:H2-M3-specific CD8 $^+$ T cells was comparable between germ-free and SPF mice (Figure S3G).

Previous work investigating responses to *Listeria monocytogenes* infection identified that H2-M3-restricted TCRs can be cross-reactive (Ploss et al., 2003). To test whether f-MIIINA:H2-M3-specific cells were cross-reactive to a previously described *Listeria*-derived H2-M3-binding fMet peptide, we utilized a previously described method of double tetramer staining (Kerksiek et al., 2001) of SLO from naive SPF mice

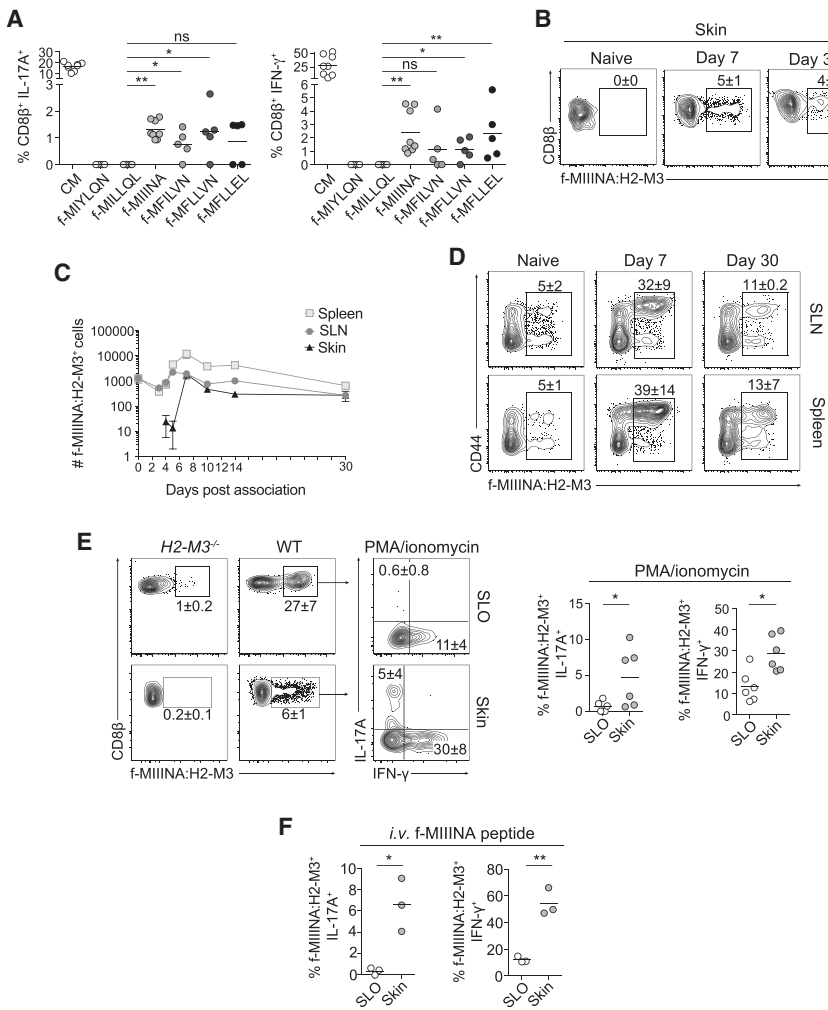


Figure 3. H2-M3-Restricted CD8 $^+$ T Cells Are Specific to *S. epidermidis*-Derived fMet Peptide Ligands

(A) *In vitro* recall of *S. epidermidis*-induced CD8 $^+$ T cells from skin with *S. epidermidis*-conditioned medium (CM) or fMet peptide-loaded splenic DCs. Frequencies of IL-17A $^+$ or IFN- γ^+ CD8 β^+ T cells after overnight culture. Splenic dendritic cells were enriched from wild-type mice.

(B–E) Frequencies (B, D, and E) and numbers (C) of f-MIIINA:H2-M3 tetramer-positive or IL-17A $^+$ or IFN- γ^+ tetramer positive (E) CD8 β^+ T cells in ear pinnae, spleen, SLNs, or pooled SLOs. Cells were isolated from naive mice or mice after indicated time-point following first *S. epidermidis* skin application (B–D). Magnetic bead-enriched spleen, SLNs, or SLOs (C–F) of intact WT (SPF) (B–F) or *H2-M3* $^{-/-}$ mice (E).

Data are represented as mean \pm SEM (C). Cells were stimulated with PMA and ionomycin (E). Mice were injected with 100 μ g f-MIIINA peptide intravenously and tissues harvested after 3 hr (F). All cells were isolated from *S. epidermidis* associated mice 2 weeks after application (E and F). Plots are gated on live CD45 $^+$ lineage $^-$ (MHCII, CD11b, $\gamma\delta$ TCR) CD90.2 $^+$ CD3 ϵ^+ CD8 β^+ T cells (B–F).

Student's t test was used to measure significance. *p < 0.05, **p < 0.005. Data are representative of 2–4 independent experiments.

See also Figure S3.

with f-MIGWII:H2-M3 and f-MIIINA:H2-M3 tetramers in the same sample and observed that staining was exclusive (Figure S3H). To address the possibility that some of the CD8 $^+$ T cells elicited by *S. epidermidis* could promiscuously respond to the 13 mitochondrial-encoded or other previously identified microbe-derived H2-M3-binding fMet peptides, we recalled *S. epidermidis* elicited CD8 $^+$ T cells *in vitro* with previously described fMet peptide epitopes derived from mitochondria or *Listeria monocytogenes* (Lindahl et al., 1997). Mitochondrial derived peptides did not significantly recall CD8 $^+$ T cells above background (Figure S3I). Thus, CD8 $^+$ T cells induced by *S. epidermidis* may not be broadly promiscuous when induced under homeostatic conditions. While we cannot exclude the possibility of cross-reactivity with other bacterial-derived fMet peptides or with mitochondrial-derived peptides during development, these results further support the idea that CD8 $^+$ T cells elicited by *S. epidermidis* skin association are specific to *S. epidermidis*-derived fMet peptides and that CD44 $^+$ f-MIIINA:H2-M3-specific cells may exist in naive mice as a result of positive selection on hematopoietic cells in the thymus as previously reported (Cho et al., 2011).

Stimulation of f-MIIINA:H2-M3-specific cells promoted IFN- γ production in all compartments analyzed at 14 days post-association (Figure 3E). Conversely, and consistent with the role of skin-derived IL-1 in licensing cytokine production in this model (Naik et al., 2012), IL-17A was only detected within the skin and IFN- γ production was significantly enhanced in both cell frequency and intensity in this compartment (Figure 3E). While IL-17A and IFN- γ production by f-MIIINA:H2-M3-specific CD8 $^+$ T cells mirrored that of the total CD8 $^+$ T cell population, tetramer staining allowed a significantly higher f-MIIINA:H2-M3-specific CD8 $^+$ T cell detection frequency (Figure 3B) than detectable via *in vitro* peptide recall (Figure 3A). As expected, f-MIIINA:H2-M3-specific cells were absent in *S. epidermidis* associated *H2-M3* $^{-/-}$ mice (Figure 3E). When f-MIIINA:H2-M3-specific CD8 $^+$ T cells were re-stimulated *in vivo* via intravenous peptide injection, we detected a similarly enhanced IL-17A and IFN- γ production within the skin compartment compared to SLO (Figure 3F). This indicates that tissue regulation of cytokine production by commensal-specific CD8 $^+$ T cells occurs proximal to T cell receptor signaling machinery.

Together, these results uncover a canonical class of bacterial antigens (fMet peptides) as potent inducers of immunity to a non-invasive microbe. Further, these results show that even in the absence of inflammation, the response to a skin microbe can be broad and systemic.

Commensal-Specific CD8⁺ T Cells Express an Immunoregulatory/Tissue-Repair Signature

Having determined that *S. epidermidis*-induced CD8⁺ T cells have a distinct cytokine profile and an unconventional MHC-I restriction, we next assessed if these cells expressed a defined transcriptional profile. To this end, we compared *S. epidermidis*-induced CD8⁺ T cells to distinct CD8⁺ T cell subsets (Tc17 and Tc1) isolated from the skin in the context of distinct infections or inflammatory states (Figure S4A). *S. epidermidis*-induced CD8⁺ T cells were isolated as CD8⁺ CCR6⁺ (Tc17) or CD8⁺ CCR6⁻ (Tc1) populations (Figure 1H). The same strategy was utilized for isolation of Tc17 and Tc1 cells from inflammatory contexts. Notably, Tc17 and Tc1 induced by topical association with *S. epidermidis* were compared to (1) CD8⁺ T cells induced by *S. epidermidis* in its pathogenic form via intradermal (i.d.) injection, consisting of exclusively Tc1 of which 50% are H2-M3-restricted (Figure S4B); (2) Tc1 cells elicited upon acute skin infection with Herpes simplex virus (HSV) (Gebhardt et al., 2009); (3) Tc1 cells elicited to skin during chronic infection with *Leishmania major* (Belkaid et al., 2002); and (4) Skin Tc17 induced in the context of experimental psoriasis triggered by treatment with the TLR7 agonist Imiquimod (Figure S4C). These multiple comparisons allowed us to control for location (skin), subset (CD8⁺ T cells), differentiation (Tc17/Tc1), inflammation (homeostasis/acute/chronic), and mode of interaction with a microbe (colonization vs. barrier breach and infection). Dendritic epidermal T cells (DETC), a population of epidermal-resident innate lymphocytes, effector memory T cells (T_{EM}), and naive CD8⁺ T cells from SLNs were also used as reference populations (Figure S4A).

We normalized isolation of cell populations post-*S. epidermidis* association and *S. epidermidis* or HSV infection at 2 weeks post-treatment. At this time point, the non-inflammatory CD8⁺ T cell response to topical *S. epidermidis* was stable (Figure 3C) and inflammation induced by HSV (van Lint et al., 2004) and i.d. *S. epidermidis* injection had resolved (Naik et al., 2015). Tc17 cells induced by Imiquimod treatment were purified at 10 days post-initial treatment and Tc1 cells induced by *L. major* skin infection were purified during the chronic stage of the infection (30 days post-infection).

Based upon global transcriptome signatures from RNA-seq, principle component analysis recapitulated the distinct nature of these T cell populations, (Figures 4A and S4D). After comparison to T_{EM} cells, we focused on transcripts either common or unique to *S. epidermidis*-induced Tc17, imiquimod-induced Tc17, and Tc1-elicited by i.d. infection with *S. epidermidis* (Figure 4B). We identified a core signature of ~1,000 genes shared among these populations (Figure 4B). When compared to Tc17 cells induced by Imiquimod, *S. epidermidis*-induced Tc17 cells differentially expressed over 2,000 genes (Figure 4C).

Next, we compared cells generated by the same microbe under steady-state or inflammatory conditions. Tc17 induced by topical association with *S. epidermidis* and Tc1 elicited by infection with *S. epidermidis* demonstrated distinct gene expression profiles, underlined by type 17 (*Rorc*, *Il17a*, *Il17f*, *Il22*, *Csf2*, *Ahr*) and type 1 (*Eomes*, *Tbx21*, *Gzma*, *Gzmb*, *Prf1*, and *Cxcr3*) signatures, respectively (Figure 4D). Of note, many of the genes elevated in *S. epidermidis*-specific Tc17 cells were associated

with immune regulation and Treg cells including the tumor necrosis factor (TNF) family members *Tnfsf4* (OX40L), *Tnfsf11* (RANKL), *Tnfsf4* (OX40), and *Tnfsf11a* (RANK); the transcription factor *Rxra* (retinoid X receptor alpha); and the transcripts for the cytokine *Il10* and the cytokine subunit *Ebi3* (IL-27 beta) (Figure 4E). Strikingly, *S. epidermidis*-elicited Tc17 cells also expressed higher levels of multiple transcripts associated with tissue repair relative to Tc1 (Figure 4F). Utilizing a curated list of tissue repair genes (Werner and Grose, 2003), we identified that *S. epidermidis*-elicited Tc17 cells were enriched in expression of a range of pleiotropic factors involved in various aspects of wound healing, such as angiogenesis (*Csf2*, *Fgf2*, *Vegfa*, *Pdgfb*), chemotaxis (*Pdgfb*, *Csf2*, *Tgfb1*, *Furin*), tissue remodeling (*Mmp10*, *Mmp25*), and extracellular matrix production (*Fgf2*, *Pdgfb*, *Tgfb1*, *Furin*) (Werner and Grose, 2003) (Figure 4F). A large number of these transcripts are factors known to affect keratinocyte proliferation: *Areg*, *Fgf2*, *Fgf16*, *Fgf18*, *Tgfb1*, *Furin*, and *Pdgfb* (Werner and Grose, 2003). Type 17, immunoregulatory and tissue repair signatures were also identified when *S. epidermidis*-specific Tc17 cells were compared to either HSV-specific Tc1 cells or topical *S. epidermidis*-specific Tc1 cells (Figure S4E).

Given the tissue repair gene signature of Tc17 cells elicited by skin colonization with *S. epidermidis*, we sought to comprehensively compare the expression of wound healing genes among all cell populations. Using principle component analysis to reduce data dimensionality, we found that the wound healing gene expression profile of Tc17 cells elicited by *S. epidermidis* was indeed distinct from all CD8⁺ T cell populations (including Imiquimod Tc17) (Figure 4G). At the global gene level as well as based on our tissue repair gene list, DETC, a population previously shown to contribute to tissue repair (Jameson et al., 2002) was also highly distinct from all other cell subsets (Figures 4H and S4D). Focused analysis of tissue repair genes expressed by *S. epidermidis*-specific Tc17 cells and DETC identified distinct expression for genes previously associated with DETC function (Figure S4F) (*Fgf7*, *Fgf10* and *Igf1*) (Nielsen et al., 2017). Additionally, we identified *Fgf2*, *Csf2*, *Mmp10*, and *Mmp25* as transcripts selectively expressed by *S. epidermidis* induced Tc17 (Figure S4G) and *Fgf16*, *Fgf18*, *Tgfb1*, *Pdgfb*, *Hmgb1*, and *Furin* as highly expressed by both *S. epidermidis* Tc17 and DETC populations (Figure S4H). Together, these results support the idea that *S. epidermidis*-elicited Tc17 cells represent a unique population and that T cells induced by commensals may contribute to tissue repair.

Commensal-Specific CD8⁺ T Cells Accelerate Wound Healing

The skin is the most exposed body surface and provides protection from mechanical injury, chemical hazard, and microbial invasion; therefore, tissue repair is of the utmost importance at this site. The tissue repair gene expression signature of CD8⁺ T cells induced by commensals prompted us to address the possibility that, in addition to their protective properties, these cells may contribute to tissue repair. A model of skin wounding induced by a punch biopsy in the ear pinnae of mice previously associated with *S. epidermidis* revealed a striking accumulation of the CD8⁺ T cells at the wound edge as shown at 3 days

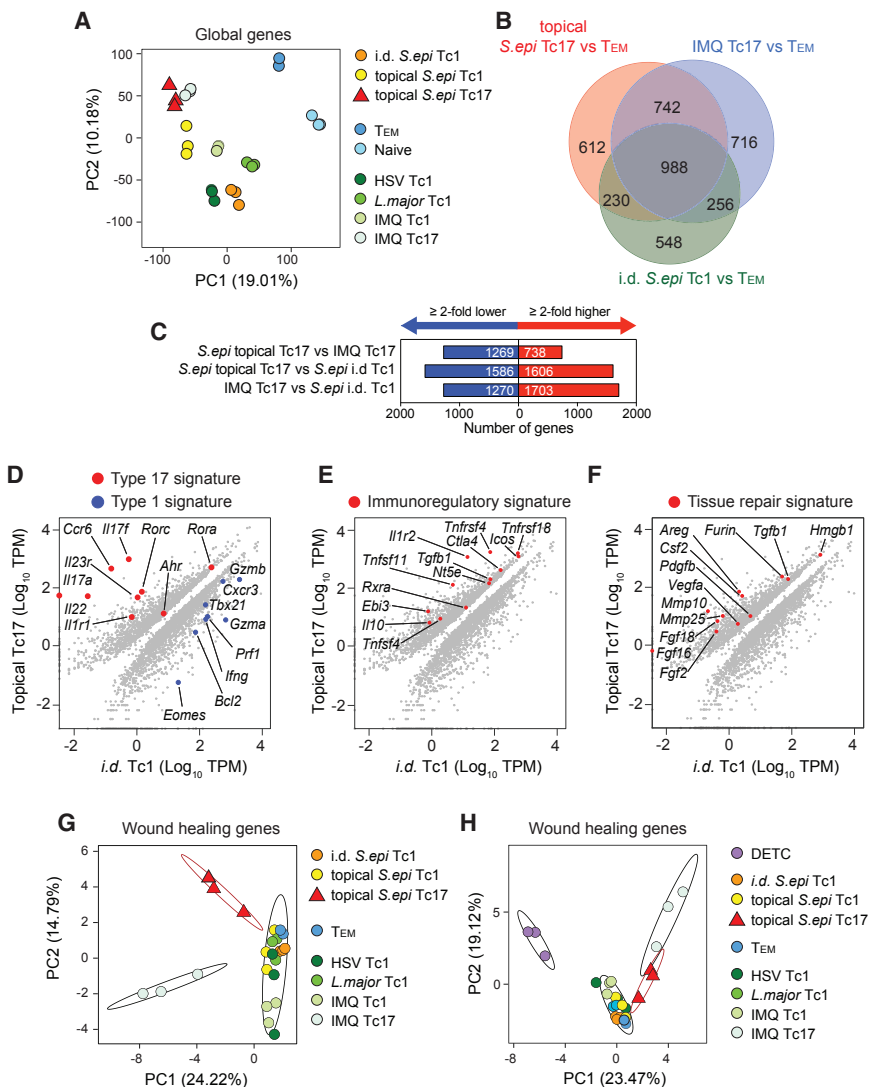


Figure 4. Commensal-Specific Tc17 Cells Are a Distinct Population and Enriched in Transcripts Associated with Immune Regulation and Tissue Repair

(A) Principle component analysis of global gene expression from cell populations identified in Figure S4A.

(B) Venn diagram from RNA-seq analysis of genes differentially expressed in pairwise comparisons between topical *S. epidermidis*-elicited Tc17, Imiquimod (IMQ)-elicited Tc17, and intradermal (i.d.) *S. epidermidis*-elicited Tc1 cells in skin relative to SLN T_{EM} cells in naive mice. Numbers of genes with greater >2-fold increase relative to T_{EM} are shown.

(C) Numbers of genes with a >2-fold increase (red) or decrease (blue) in expression levels between the indicated populations.

(D–F) Diagonal plots showing differentially expressed genes (>2-fold, $P_{adj} < 0.05$) comparing topical *S. epidermidis*-elicited Tc17 to i.d. *S. epidermidis*-elicited Tc1 cells in skin for Type 17/Type 1 (D), immunoregulatory (E), and tissue repair (F) signatures.

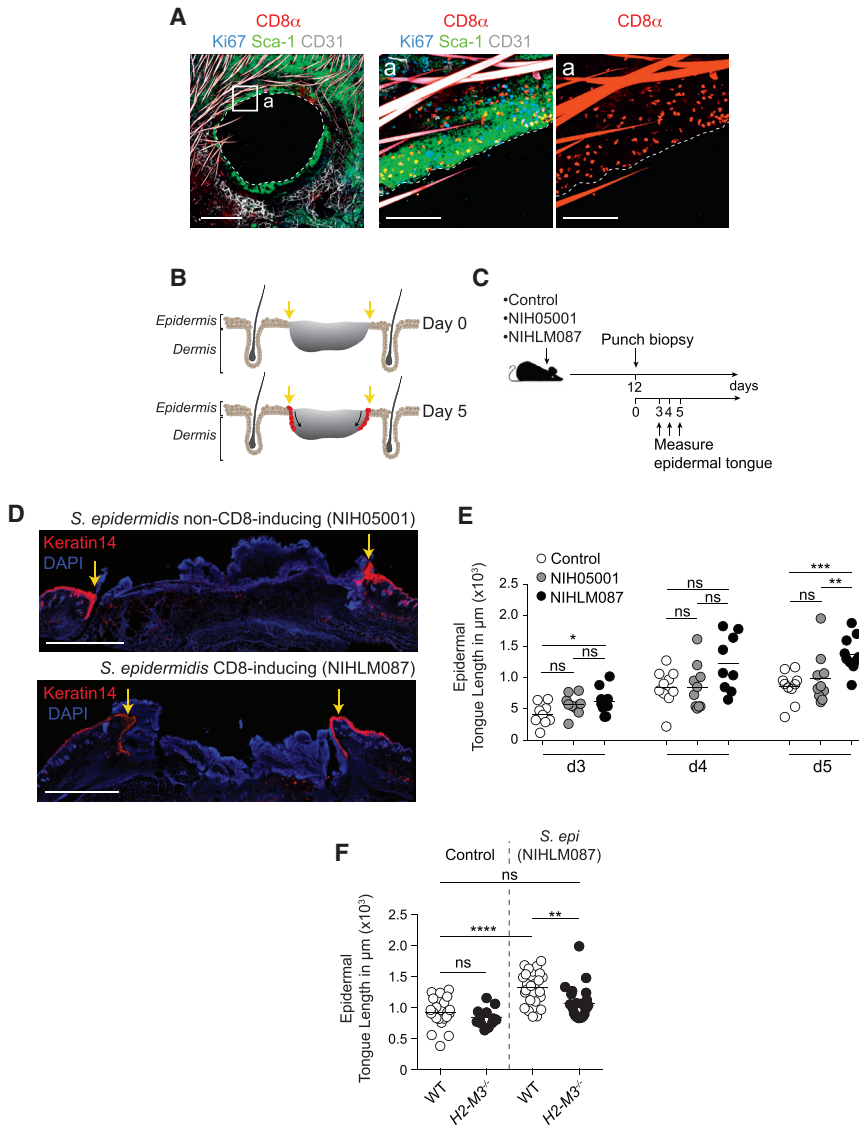
(G and H) Principle component analysis of curated wound healing gene expression from cell populations identified in Figure S4A without (G) and with DETC (H). Ellipses denote 95% confidence intervals of the mean of selected cell populations: topical *S. epidermidis*-elicited Tc17, IMQ-elicited Tc17, DETC, and all others.

See also Figure S4.

post-injury (Figure 5A). Next, we utilized an approach of backskin punch biopsy that allows precise quantification of repair (Keyes et al., 2016). In this model, progression of the healing wound can be measured via the length of the proliferating epidermal keratinocyte tongue that migrates into the wound bed over time, eventually resulting in wound closure (Figure 5B). Wounds were performed at 12 days post-association with *S. epidermidis* (NIHLM087), a time point near the peak of the CD8⁺ T cell response with sustained low bacterial burden (Figure S5A). To control for bacterial exposure and potential innate immunity contribution (Lai et al., 2010), we included a group associated with a non-CD8-inducing *S. epidermidis* strain (NIH05001) (Figures 1C and 5C). Wounds were measured 3, 4, and 5 days post-wounding, a time span that was previously shown to have the highest re-epithelialization activity (Keyes et al., 2016) (Figure 5C). We identified significant differences in basal keratinocyte epidermal tongue length on day 3 and 5 between wounds in mice that were previously associated with the CD8⁺ T cell inducing

S. epidermidis strain as compared to one or more control groups (Figures 5D and 5E). Thus, *S. epidermidis*-induced CD8⁺ T cells promoted more rapid epidermal keratinocyte tongue progression and therefore accelerated wound healing. This response was independent of the presence of DETC (Figure S5B). Accelerated healing was not associated

with changes in inflammatory infiltrates between mice associated with CD8-inducing or non-inducing strains (Figure S5C). To assess the contribution of *S. epidermidis*-induced CD8⁺ T cells to this process, we measured epidermal tongue length in wounds of WT and H2-M3 deficient mice that were previously topically associated with *S. epidermidis*. The ability of *S. epidermidis* to accelerate this process was significantly reduced in H2-M3^{−/−} mice formally linking non-classical MHCI restricted cells, the microbiota, and tissue repair (Figure 5F). Differences in tissue repair between WT and H2-M3^{−/−} mice was not associated with changes in skin hematopoietic cell infiltrate (Figure S5D), but with a transient and discrete change in tissue gene expression associated with muscle responses (Figures S5E and S5F) supporting the idea that at least one of the targets of this process may be the arrector pilo muscles (Torkamani et al., 2017). Together, these results identify an important role for commensal-specific, H2-M3-restricted CD8⁺ T cells in driving enhanced tissue repair.



medium (control) or NIHLM087. Tongue lengths were measured at 5 days after backskin punch biopsy. Student's t test was used to measure significance. * $p < 0.05$, ** $p < 0.005$, *** $p < 0.0005$, and **** $p < 0.0001$. Data are representative of 2–4 independent experiments.

See also Figure S5.

DISCUSSION

Most of what we understand today about the function of the immune system comes from the exploration of responses to pathogenic microbes. However, the vast majority of immune system-microbial encounters are those resulting from the symbiotic relationship with the microbiota (Belkaid and Hand, 2014). Here, we show that this fundamental class of immunity can promote an immune-microbe dialog endowed with pleiotropic functions.

Our present results propose that the symbiotic dialog between the microbiota and the immune system could be dominantly mediated by non-classical MHC molecules. Non-polymorphic MHC representatives, referred to as non-classical MHC for those

Figure 5. Commensal-Specific CD8 $^{+}$ T Cells Accelerate Wound Healing

(A) Representative imaging of whole-mount ear pinnae at 3 days after 2.5-mm ear punch biopsy from mice (15 days post-initial *S. epidermidis* association). Whole-mounts were stained for CD8 $^{+}$ T cells (CD8 α), keratinocytes (Sca-1), blood vessels (CD31), and cycling cells (Ki67) and imaged by confocal microscopy. Scale bars, 150, 1,000, and 1,000 μm , respectively. Hair is autofluorescent in CD8 α and CD31 channels.

(B) Schematic depicting progress of re-epithelialization over time after wounding. Yellow arrows denote wound edge. Red indicates advancing epidermal tongue of basal keratinocytes that stains brightly for keratin 14.

(C) Mice were topically associated with growth medium alone (control), non-CD8 $^{+}$ T cell-inducing *S. epidermidis* isolate (NIH05001), or CD8 $^{+}$ T cell-inducing *S. epidermidis* isolate (NIHLM087) followed by a backskin punch biopsy 12 days later. Epidermal keratinocyte tongue length was measured at days 3, 4, and 5 post-wounding.

(D) Immunofluorescence images of backskin wounds at day 5 after punch biopsy. Sections are immunolabeled for basal epidermal keratinocytes (Keratin 14) and co-stained with DAPI. Scale bars, 1,000 μm . Yellow arrows denote wound edge.

(E) Quantification of the length of the tongue of epidermal keratinocytes that migrate in from the wound edges during re-epithelialization of the wound bed in WT mice. Mice were topically skin associated with growth medium (control), a non-CD8 $^{+}$ T cell-inducing *S. epidermidis* (NIH05001) strain or a CD8 $^{+}$ T cell-inducing *S. epidermidis* (NIHLM087) strain. Tongue lengths were measured at 3–5 days after backskin punch biopsy

(F) Quantification of the length of the tongue of epidermal keratinocytes that migrate in from the wound edges during re-epithelialization of the wound bed in WT or H2-M3 $^{-/-}$ mice. Mice were topically skin associated with growth

encoded by genes located within the MHC region and MHC-like molecules for those outside the MHC, exist for both class I and class II proteins, the most diverse being those related to the MHC class I molecules (Adams and Luoma, 2013). While these molecules have been shown to contribute to the recognition of pathogenic microbes, a protective role for these responses has only recently been addressed (Seaman et al., 2000; Shang et al., 2016; Van Rhijn et al., 2015). Our present results propose that non-classical MHC molecules may have been dominantly maintained as a means to engage in a dialog with the microbiota. In support of this, barrier sites are enriched in cells restricted to non-classical MHC presentation including natural killer (NK) cells, natural killer T (NKT) cells, $\gamma\delta$ T cells, mucosal associated

invariant T (MAIT) cells (Fan and Rudensky, 2016), and, as shown here, H2-M3-restricted CD8⁺ T cells. Although previous work has identified that H2-M3-restricted TCRs can be promiscuous (Ploss et al., 2003), our work supports the idea that commensal-specific H2-M3-restricted CD8⁺ T cells, at least under conditions of homeostatic immunity, may not be as cross-reactive.

While our present results highlight a role for H2-M3 in mice, it has been suggested that an analog may exist in humans. Precedence for this comes from the identification of the analog to the mouse MHC Ib molecule Qa-1 in humans, which was identified as human leukocyte antigen-E (HLA-E). These two molecules have little amino acid sequence homology, yet bind similar peptides (Rodgers and Cook, 2005). Further, many non-classical MHC I molecules exist in humans that may serve a similar purpose. Intriguingly, association of non-human primate skin with *S. epidermidis* was sufficient to significantly enhance skin Tc17. The nature of the potential MHC I involved in such settings remains to be identified.

Of particular relevance to our present observation, MHC Ib-restricted immune cell populations have been shown to be enriched at barrier sites during early life (Gensollen et al., 2016), a time of extraordinary and dynamic exposure to the microbiota. For instance, bacteria derived sphingolipids can interact via non-classical CD1d molecules with NKT cells early in life, a response that shapes subsequent susceptibility to inflammation (An et al., 2014). The ability of MHC Ib molecules to present antigens with specific motifs, which can be derived from a large constituency of the microbiota, place immune cells that recognize them as ideal candidates for the constitutive sensing and recognition of microbiota-derived antigens or metabolites.

One remarkable feature of the CD8⁺ T cells induced by *S. epidermidis* is their unusual and complex signature that distinguishes them from canonical CD8⁺ T cells. Whether this unique phenotype results from the engagement of MHC Ib molecules or the non-inflammatory setting surrounding these responses remains to be addressed. Nonetheless, we can speculate that induction of immunity under homeostatic conditions may poised cells to develop a less polarized phenotype and may sustain the development of pleiotropic programs. Notably, CD8⁺ T cells induced by *S. epidermidis* express a high number of transcripts associated with tissue repair compared to CD8⁺ T cells induced by pathogenic encounter and were able to promote skin repair. In the skin, tissue repair is of the utmost importance and complex and redundant pathways converge to promote this vital process. For instance, DETC were also previously shown to promote tissue repair (Nielsen et al., 2017) but were not required for the tissue repair effect of *S. epidermidis*, supporting the idea that these two cell subsets play distinct roles in this process. A link between the microbiota and tissue repair was previously provided by the observation that, in the gut, TLR activation by commensals was required to promote tissue repair and host survival following acute injury (Rakoff-Nahoum et al., 2004). In the skin, a defined product of *S. epidermidis*, lipoteichoic acid (LTA), can also mitigate inflammation via its capacity to bind to Toll-like receptor (TLR) 2, thereby promoting wound healing (Lai et al., 2009). While we do not exclude a synergistic role for this molecule, in our setting we found that *S. epidermidis*

(NIH05001) decorated with LTA, but unable to induce CD8⁺ T cells failed to promote tissue repair. Of interest, no differences in cellular recruitment were observed in the presence or absence of H2-M3 molecules post-injury in the context of *S. epidermidis* suggesting that T cells induced by this commensal may target the non-hematopoietic compartment. The impact of CD8⁺ T cells induced by *S. epidermidis* was detectable during the proliferation phase of wound healing, perhaps through an effect on keratinocyte proliferation. Notably, CD8⁺ T cells induced by *S. epidermidis* express high levels of amphiregulin, a molecule described for its mitogenic role on keratinocytes through binding the epidermal growth factor receptor (EGFR) (Werner and Grose, 2003). Additionally, these cells expressed fibroblast growth factor (FGF) family members with previously identified roles as keratinocyte mitogens (Kawano et al., 2005; Werner and Grose, 2003). This production of an EGFR ligand and FGFs by commensal-specific CD8⁺ T cells supports the idea that these cells may utilize redundant mechanisms to promote tissue repair. We also found that CD8⁺ T cells induced by *S. epidermidis* localized to the edge of the wound post-injury, a tropism that may serve the dual purpose of enhancing keratinocyte proliferation while at the same time promoting antimicrobial defense at a site of high vulnerability. In addition to keratinocytes, our results support the idea that *S. epidermidis*-induced CD8⁺ T cells may also impact the skin muscle compartment. The skin is enriched in *arrector pili* muscles that are attached to hair follicles and these muscles have been proposed to contribute to the maintenance of hair follicle integrity (Torkamani et al., 2017). How commensal-specific T cells restore the function of these structures and how such process contribute to tissue repair remains to be addressed.

There are at least two possible mechanisms to explain how commensal-specific CD8⁺ T cells are able to sense and respond to tissue injury. The first could be in an innate manner, through binding of signal molecules to receptors other than the TCR, the other could be through TCR binding to *S. epidermidis* fMet peptide:H2-M3 ligands made available via barrier breach. Such phenomenon may be applicable to a large fraction of cells residing at barrier sites. Indeed, because of the extraordinary number of potential antigens expressed by the microbiota, a significant fraction of resident lymphocytes including non-conventional lymphocytes are expected to be microbiota specific. Consequently, any barrier breach mediated by infection or injury is likely to occur in the context of a much broader recall response against diverse microbial antigens (Hand et al., 2012), a response that as we show here could also contribute to tissue repair.

Together, our work proposes that the rules and properties of immunity to the microbiota are distinct from those induced by pathogenic encounters. Here, we uncover some defining features of commensal-specific immunity, a pleiotropic class of immunity that we show to be highly entwined with tissue physiology. These findings may have important clinical implications. Indeed, despite the importance of healing for host survival, mechanisms underpinning tissue repair and its failure to heal are still poorly understood and current therapies are limited (Eming et al., 2014). As such, poor wound healing after trauma, surgery, acute illness, or chronic disease conditions remains a

serious public health concern (Eming et al., 2014). In this context, by uncovering a link between commensal-specific immunity/non-classical MHC and tissue repair, our work may open the door to novel therapeutic interventions based on the physiological integration of host microbiota interactions.

STAR★METHODS

Detailed methods are provided in the online version of this paper and include the following:

- KEY RESOURCES TABLE
- CONTACT FOR REAGENT AND RESOURCE SHARING
- EXPERIMENTAL MODEL AND SUBJECT DETAILS
 - Mice
 - Non-human primates
- METHODS DETAILS
 - Topical association and intradermal infection of mice with *Staphylococcus* species
 - *Leishmania* major and herpes simplex virus type 1 (HSV-1) skin infections
 - Imiquimod induced psoriasis-like dermatitis
 - Non-human primate skin and association with *S. epidermidis*
 - *S. epidermidis* conditioned medium preparation
 - Tissue processing
 - Wounding study
 - Immunofluorescence/confocal microscopy of ear pinnae
 - Immunofluorescence/epifluorescence microscopy of backskin wounds
 - *In vitro* re-stimulation
 - Phenotypic analysis
 - *In vivo* recall of f-MIIINA:H2-M3-specific CD8⁺ T cells via intravenous peptide injection
 - Cell enrichment
 - DC-T cell co-culture assay
 - T cell isolation and RNA extraction for RNA-sequencing
 - RNA library preparation and sequencing
 - Whole tissue RNA-sequencing and transcriptome analysis
- QUANTIFICATION AND STATISTICAL ANALYSIS
 - Statistical analysis
- DATA AND SOFTWARE AVAILABILITY

SUPPLEMENTAL INFORMATION

Supplemental Information includes five figures and can be found with this article online at <https://doi.org/10.1016/j.cell.2017.12.033>.

ACKNOWLEDGMENTS

This work was supported by the Division of Intramural Research of the NIAID, 1ZIAAI0011150 NCI, ZIABC01115309 NIAMS, ZIAAR04115910 and NIDDK ZIADK05451611. J.L.L. was supported by the NIGMS Postdoctoral Research Associate (PRAT) fellowship program. O.J.H. was supported by a National Psoriasis Foundation Early Career Research Grant. S.T. was supported by a Long-Term EMBO Fellowship. We thank the NIAID animal facility staff; the NIAID Microbiome Program gnotobiotic animal facility for the use of germ-

free mice; K. Holmes, C. Eigsti, T. Hawley, and E. Stregevsky (NIAID Flow Cytometry facility); O. Schwartz (NIAID Biological Imaging facility), K. Beacht, J. LeGrand, and J. Davis for technical assistance; R. Bosselut for the *B2m*^{-/-} mice; and H. Cantor for the *Qa-1*^{-/-} mice. We thank the NIH tetramer core facility (Emory University) for provision of fMet peptide:H2-M3 tetramers. We thank all the members of the Belkaid laboratory for critically reading the manuscript and helpful discussions.

AUTHOR CONTRIBUTIONS

J.L.L. and Y.B. designed the studies and wrote the manuscript. J.L.L. performed the experiments and analyzed the data. O.J.H., S.-J.H., and N.B. participated in performing the experiments, provided intellectual expertise, and helped to interpret the experimental results. I.V.-C., A.L.B., A.V.V., J.J.O., S.K.S., J.S., A.D., G.T., J.H.A., and T.M.K. assisted with the RNA-seq study. S.P.R. and B.R. assisted with the wild mouse study. S.-J.H. and S.T. performed whole-tissue mount imaging studies. M.S. and N.C. assisted with the wound imaging studies. O.J.H., S.-J.H., C.-R.W., and N.B. assisted with manuscript preparation. J.M.B. provided primate tissues and guidance on the preparation and staining. All authors read and commented on the manuscript.

DECLARATION OF INTERESTS

The authors declare no competing interests.

Received: March 20, 2017

Revised: October 17, 2017

Accepted: December 21, 2017

Published: January 18, 2018

REFERENCES

- Adams, E.J., and Luoma, A.M. (2013). The adaptable major histocompatibility complex (MHC) fold: structure and function of nonclassical and MHC class I-like molecules. *Annu. Rev. Immunol.* 31, 529–561.
- An, D., Oh, S.F., Olszak, T., Neves, J.F., Avci, F.Y., Erturk-Hasdemir, D., Lu, X., Zeissig, S., Blumberg, R.S., and Kasper, D.L. (2014). Sphingolipids from a symbiotic microbe regulate homeostasis of host intestinal natural killer T cells. *Cell* 156, 123–133.
- Anders, S., and Huber, W. (2010). Differential expression analysis for sequence count data. *Genome Biol.* 11, R106.
- Belkaid, Y., and Hand, T.W. (2014). Role of the microbiota in immunity and inflammation. *Cell* 157, 121–141.
- Belkaid, Y., and Segre, J.A. (2014). Dialogue between skin microbiota and immunity. *Science* 346, 954–959.
- Belkaid, Y., and Tamoutounour, S. (2016). The influence of skin microorganisms on cutaneous immunity. *Nat. Rev. Immunol.* 16, 353–366.
- Belkaid, Y., Von Stebut, E., Mendez, S., Lira, R., Caler, E., Bertholet, S., Udey, M.C., and Sacks, D. (2002). CD8⁺ T cells are required for primary immunity in C57BL/6 mice following low-dose, intradermal challenge with *Leishmania* major. *J. Immunol.* 168, 3992–4000.
- Beura, L.K., Hamilton, S.E., Bi, K., Schenkel, J.M., Odumade, O.A., Casey, K.A., Thompson, E.A., Fraser, K.A., Rosato, P.C., Filali-Mouhim, A., et al. (2016). Normalizing the environment recapitulates adult human immune traits in laboratory mice. *Nature* 532, 512–516.
- Bolger, A.M., Lohse, M., and Usadel, B. (2014). Trimmomatic: a flexible trimmer for Illumina sequence data. *Bioinformatics* 30, 2114–2120.
- Byrd, A.L., Deming, C., Cassidy, K.B., Harrison, O.J., Conlan, S., Belkaid, Y., Segre, J.A., and Kong, H.H.; NISC Comparative Sequencing Program (2017). *Staphylococcus aureus* and *S. epidermidis* strain diversity underlying human atopic dermatitis. *Sci. Transl. Med.* 9, pii: eaal465.
- Cho, H., Bediako, Y., Xu, H., Choi, H.J., and Wang, C.R. (2011). Positive selecting cell type determines the phenotype of MHC class Ib-restricted CD8⁺ T cells. *Proc. Natl. Acad. Sci. USA* 108, 13241–13246.

- Chun, T., Serbina, N.V., Nolt, D., Wang, B., Chiu, N.M., Flynn, J.L., and Wang, C.R. (2001). Induction of M3-restricted cytotoxic T lymphocyte responses by N-formylated peptides derived from *Mycobacterium tuberculosis*. *J. Exp. Med.* 193, 1213–1220.
- Cong, Y., Feng, T., Fujihashi, K., Schoeb, T.R., and Elson, C.O. (2009). A dominant, coordinated T regulatory cell-IgA response to the intestinal microbiota. *Proc. Natl. Acad. Sci. USA* 106, 19256–19261.
- Conlan, S., Mijares, L.A., Becker, J., Blakesley, R.W., Bouffard, G.G., Brooks, S., Coleman, H., Gupta, J., Gurson, N., Park, M., et al.; NISC Comparative Sequencing Program (2012). *Staphylococcus epidermidis* pan-genome sequence analysis reveals diversity of skin commensal and hospital infection-associated isolates. *Genome Biol.* 13, R64.
- Dobin, A., Davis, C.A., Schlesinger, F., Drenkow, J., Zaleski, C., Jha, S., Batut, P., Chaisson, M., and Gingeras, T.R. (2013). STAR: ultrafast universal RNA-seq aligner. *Bioinformatics* 29, 15–21.
- Doyle, C.K., Davis, B.K., Cook, R.G., Rich, R.R., and Rodgers, J.R. (2003). Hyperconservation of the N-formyl peptide binding site of M3: evidence that M3 is an old eutherian molecule with conserved recognition of a pathogen-associated molecular pattern. *J. Immunol.* 171, 836–844.
- Eming, S.A., Martin, P., and Tomic-Canic, M. (2014). Wound repair and regeneration: mechanisms, signaling, and translation. *Sci. Transl. Med.* 6, 265sr6.
- Ewels, P., Magnusson, M., Lundin, S., and Käller, M. (2016). MultiQC: summarize analysis results for multiple tools and samples in a single report. *Bioinformatics* 32, 3047–3048.
- Fan, X., and Rudensky, A.Y. (2016). Hallmarks of Tissue-Resident Lymphocytes. *Cell* 164, 1198–1211.
- Gebhardt, T., Wakim, L.M., Eidsmo, L., Reading, P.C., Heath, W.R., and Carbone, F.R. (2009). Memory T cells in nonlymphoid tissue that provide enhanced local immunity during infection with herpes simplex virus. *Nat. Immunol.* 10, 524–530.
- Gensollen, T., Iyer, S.S., Kasper, D.L., and Blumberg, R.S. (2016). How colonization by microbiota in early life shapes the immune system. *Science* 352, 539–544.
- Godfrey, D.I., Uldrich, A.P., McCluskey, J., Rossjohn, J., and Moody, D.B. (2015). The burgeoning family of unconventional T cells. *Nat. Immunol.* 16, 1114–1123.
- Hand, T.W., Dos Santos, L.M., Bouladoux, N., Molloy, M.J., Pagán, A.J., Pepper, M., Maynard, C.L., Elson, C.O., 3rd, and Belkaid, Y. (2012). Acute gastrointestinal infection induces long-lived microbiota-specific T cell responses. *Science* 337, 1553–1556.
- Honda, K., and Littman, D.R. (2016). The microbiota in adaptive immune homeostasis and disease. *Nature* 535, 75–84.
- Ivanov, I.I., Atarashi, K., Manel, N., Brodie, E.L., Shima, T., Karaoz, U., Wei, D., Goldfarb, K.C., Santee, C.A., Lynch, S.V., et al. (2009). Induction of intestinal Th17 cells by segmented filamentous bacteria. *Cell* 139, 485–498.
- Jameson, J., Ugarte, K., Chen, N., Yachi, P., Fuchs, E., Boismenu, R., and Havran, W.L. (2002). A role for skin gammadele T cells in wound repair. *Science* 296, 747–749.
- Kawano, M., Komi-Kuramochi, A., Asada, M., Suzuki, M., Oki, J., Jiang, J., and Imamura, T. (2005). Comprehensive analysis of FGF and FGFR expression in skin: FGF18 is highly expressed in hair follicles and capable of inducing anagen from telogen stage hair follicles. *J. Invest. Dermatol.* 124, 877–885.
- Kerksiek, K.M., Busch, D.H., and Pamer, E.G. (2001). Variable immunodominance hierarchies for H2-M3-restricted N-formyl peptides following bacterial infection. *J. Immunol.* 166, 1132–1140.
- Keyes, B.E., Liu, S., Asare, A., Naik, S., Levorse, J., Polak, L., Lu, C.P., Nikolicova, M., Pasolli, H.A., and Fuchs, E. (2016). Impaired epidermal to dendritic T cell signaling slows wound repair in aged skin. *Cell* 167, 1323–1338.e14.
- Lai, Y., Di Nardo, A., Nakatsuji, T., Leichtle, A., Yang, Y., Cogen, A.L., Wu, Z.R., Hooper, L.V., Schmidt, R.R., von Aulock, S., et al. (2009). Commensal bacteria regulate Toll-like receptor 3-dependent inflammation after skin injury. *Nat. Med.* 15, 1377–1382.
- Lai, Y., Cogen, A.L., Radek, K.A., Park, H.J., Macleod, D.T., Leichtle, A., Ryan, A.F., Di Nardo, A., and Gallo, R.L. (2010). Activation of TLR2 by a small molecule produced by *Staphylococcus epidermidis* increases antimicrobial defense against bacterial skin infections. *J. Invest. Dermatol.* 130, 2211–2221.
- Li, B., and Dewey, C.N. (2011). RSEM: accurate transcript quantification from RNA-seq data with or without a reference genome. *BMC Bioinformatics* 12, 323.
- Lindahl, K.F., Byers, D.E., Dabhi, V.M., Hovik, R., Jones, E.P., Smith, G.P., Wang, C.R., Xiao, H., and Yoshino, M. (1997). H2-M3, a full-service class Ib histocompatibility antigen. *Annu. Rev. Immunol.* 15, 851–879.
- Moon, J.J., Chu, H.H., Pepper, M., McSorley, S.J., Jameson, S.C., Kedl, R.M., and Jenkins, M.K. (2007). Naive CD4(+) T cell frequency varies for different epitopes and predicts repertoire diversity and response magnitude. *Immunity* 27, 203–213.
- Naik, S., Bouladoux, N., Wilhelm, C., Molloy, M.J., Salcedo, R., Kastenmuller, W., Deming, C., Quinones, M., Koo, L., Conlan, S., et al. (2012). Compartmentalized control of skin immunity by resident commensals. *Science* 337, 1115–1119.
- Naik, S., Bouladoux, N., Linehan, J.L., Han, S.J., Harrison, O.J., Wilhelm, C., Conlan, S., Himmelfarb, S., Byrd, A.L., Deming, C., et al. (2015). Commensal-dendritic-cell interaction specifies a unique protective skin immune signature. *Nature* 520, 104–108.
- Nielsen, M.M., Witherden, D.A., and Havran, W.L. (2017). $\gamma\delta$ T cells in homeostasis and host defence of epithelial barrier tissues. *Nat. Rev. Immunol.* 17, 733–745.
- Obar, J.J., Khanna, K.M., and Lefrançois, L. (2008). Endogenous naive CD8+ T cell precursor frequency regulates primary and memory responses to infection. *Immunity* 28, 859–869.
- Pamer, E.G. (2016). Resurrecting the intestinal microbiota to combat antibiotic-resistant pathogens. *Science* 352, 535–538.
- Ploss, A., Lauvau, G., Contos, B., Kerksiek, K.M., Guirnalda, P.D., Leiner, I., Lenz, L.L., Bevan, M.J., and Pamer, E.G. (2003). Promiscuity of MHC class Ib-restricted T cell responses. *J. Immunol.* 171, 5948–5955.
- Rakoff-Nahoum, S., Paglino, J., Eslami-Varzaneh, F., Edberg, S., and Medzhitov, R. (2004). Recognition of commensal microflora by toll-like receptors is required for intestinal homeostasis. *Cell* 118, 229–241.
- Rodgers, J.R., and Cook, R.G. (2005). MHC class Ib molecules bridge innate and acquired immunity. *Nat. Rev. Immunol.* 5, 459–471.
- Scharschmidt, T.C., Vasquez, K.S., Truong, H.A., Gearty, S.V., Pauli, M.L., Nosbaum, A., Gratz, I.K., Otto, M., Moon, J.J., Liese, J., et al. (2015). A wave of regulatory T cells into neonatal skin mediates tolerance to commensal microbes. *Immunity* 43, 1011–1021.
- Schenkel, J.M., and Masopust, D. (2014). Tissue-resident memory T cells. *Immunity* 41, 886–897.
- Seaman, M.S., Wang, C.R., and Forman, J. (2000). MHC class Ib-restricted CTL provide protection against primary and secondary *Listeria monocytogenes* infection. *J. Immunol.* 165, 5192–5201.
- Shang, S., Siddiqui, S., Bian, Y., Zhao, J., and Wang, C.R. (2016). Nonclassical MHC Ib-restricted CD8+ T cells recognize *mycobacterium tuberculosis*-derived protein antigens and contribute to protection against infection. *PLoS Pathog.* 12, e1005688.
- Torkamani, N., Rufaut, N., Jones, L., and Sinclair, R. (2017). The arrector pili muscle, the bridge between the follicular stem cell niche and the interfollicular epidermis. *Anat. Sci. Int.* 92, 151–158.
- van der Fits, L., Mourits, S., Voerman, J.S., Kant, M., Boon, L., Laman, J.D., Cornelissen, F., Mus, A.M., Florencia, E., Prens, E.P., and Lubberts, E. (2009). Imiquimod-induced psoriasis-like skin inflammation in mice is mediated via the IL-23/IL-17 axis. *J. Immunol.* 182, 5836–5845.
- van Lint, A., Ayers, M., Brooks, A.G., Coles, R.M., Heath, W.R., and Carbone, F.R. (2004). Herpes simplex virus-specific CD8+ T cells can clear established lytic infections from skin and nerves and can partially limit the early spread of virus after cutaneous inoculation. *J. Immunol.* 172, 392–397.

- Van Rhijn, I., Godfrey, D.I., Rossjohn, J., and Moody, D.B. (2015). Lipid and small-molecule display by CD1 and MR1. *Nat. Rev. Immunol.* **15**, 643–654.
- Vugmeyster, Y., Glas, R., Pérarnau, B., Lemonnier, F.A., Eisen, H., and Ploegh, H. (1998). Major histocompatibility complex (MHC) class I KbDb β -deficient mice possess functional CD8+ T cells and natural killer cells. *Proc. Natl. Acad. Sci. USA* **95**, 12492–12497.
- Werner, S., and Grose, R. (2003). Regulation of wound healing by growth factors and cytokines. *Physiol. Rev.* **83**, 835–870.
- Yang, Y., Torchinsky, M.B., Gobert, M., Xiong, H., Xu, M., Linehan, J.L., Alonzo, F., Ng, C., Chen, A., Lin, X., et al. (2014). Focused specificity of intestinal TH17 cells towards commensal bacterial antigens. *Nature* **510**, 152–156.

STAR★METHODS**KEY RESOURCES TABLE**

REAGENT or RESOURCE	SOURCE	IDENTIFIER
Antibodies		
Anti-mouse CCR6, PE (29-2L17)	Biolegend	Cat# 129804 RRID: AB_1279137
Anti-mouse CD3 ϵ , PerCP-Cy5.5 (145-2C11)	eBioscience	Cat# 45-0031-82 RRID: AB_1107000
Anti-mouse CD3 ϵ , BV605 (145-2C11)	Biolegend	Cat# 100351 RRID: AB_2565842
Anti-mouse CD4, AF700 (RM4-5)	eBioscience	Cat# 56-0042-82 RRID: AB_494000
Anti-mouse CD4, BV605 (RM4-5)	Biolegend	Cat# 100548 RRID: AB_2563054
Anti-mouse CD8 α , PE (53-6.7)	eBioscience	Cat# 12-0081-83 RRID: AB_465531
Anti-mouse CD8 β , FITC (eBioH35-17.2)	eBioscience	Cat# 11-0083-82 RRID: AB_657764
Anti-mouse CD8 β , PE-Cy7 (eBioH35-17.2)	eBioscience	Cat# 25-0083-82 RRID: AB_11218494
Anti-mouse CD8 β , eFluor 450 (eBioH35-17.2)	eBioscience	Cat# 48-0083-82 RRID: AB_11218504
Anti-mouse CD11b, PE-CF594 (M1/70)	BD Biosciences	Cat# 562287 RRID: AB_11154216
Anti-mouse CD11b, eFluor 450 (M1/70)	eBioscience	Cat# 48-0112-82 RRID: AB_1582236
Anti-mouse CD11b, BV605 (M1/70)	Biolegend	Cat# 101257 RRID: AB_2565431
Anti-mouse CD11b, BV785 (M1/70)	Biolegend	Cat# 101243 RRID: AB_2561373
Anti-mouse CD11c, APC-eFluor 780 (N418)	eBioscience	Cat# 47-0114-82 RRID: AB_1548652
Anti-mouse CD11c, eFluor 450 (N418)	eBioscience	Cat# 48-0114-82 RRID: AB_1548654
Anti-mouse CD11c, BV785 (N418)	Biolegend	Cat# 117335 RRID: AB_11219204
Anti-mouse CD16/32 (2.4G2)	Bio-X-Cell	Cat# CUS-HB-197 RRID: AB_2687830
Anti-mouse CD19, PE/Dazzle 594 (6D5)	Biolegend	Cat# 115553 RRID: AB_2564000
Anti-mouse CD19, eFluor 450 (1D3)	eBioscience	Cat# 48-0193-82 RRID: AB_2043815
Anti-mouse CD24, FITC (M1/69)	Biolegend	Cat# 101806 RRID: AB_312839
Anti-mouse CD31, APC (390)	Biolegend	Cat# 102410 RRID: AB_312905

(Continued on next page)

Continued

REAGENT or RESOURCE	SOURCE	IDENTIFIER
Anti-mouse CD44, PE-Cy7 (IM7)	eBioscience	Cat# 25-0441-82 RRID: AB_469623
Anti-mouse CD44, AF700 (IM7)	eBioscience	Cat# 56-0441-82 RRID: AB_494011
Anti-mouse CD45, APC-eFluor 780 (30-F11)	eBioscience	Cat# 47-0451-82 RRID: AB_1548781
Anti-mouse CD45, BV510 (30-F11)	Biolegend	Cat# 103138 RRID: AB_2563061
Anti-mouse CD45.1, FITC (A20)	eBioscience	Cat# 11-0453-85 RRID: AB_465059
Anti-mouse CD45.1, BV510 (A20)	Biolegend	Cat# 110741 RRID: AB_2563378
Anti-mouse CD45.2, APC-eFluor 780 (104)	eBioscience	Cat# 47-0454-82 RRID: AB_1272175
Anti-mouse CD49f, eFluor 450 (eBioGoH3)	eBioscience	Cat# 48-0495-82 RRID: AB_11042564
Anti-mouse CD62L, FITC (MEL-14)	eBioscience	Cat# 11-0621-85 RRID: AB_465110
Anti-mouse CD64, PerCP-Cy5.5 (X54-5/7.1)	Biolegend	Cat# 139308 RRID: AB_2561963
Anti-mouse CD64, BV421 (X54-5/7.1)	Biolegend	Cat# 139309 RRID: AB_2562694
Anti-mouse CD69, APC (H1.2F3)	Biolegend	Cat# 104514 RRID: AB_492843
Anti-mouse CD90.2, BV605 (53-2.1)	Biolegend	Cat# 140318 RRID: AB_2650924
Anti-mouse CD90.2, BV785 (30-H12)	Biolegend	Cat# 105331 RRID: AB_2562900
Anti-mouse CD103, PerCP-eFluor 710 (2E7)	eBioscience	Cat# 46-1031-82 RRID: AB_2573704
Anti-mouse CD122, PerCP-eFluor 710 (TM-b1)	eBioscience	Cat# 46-1222-82 RRID: AB_11064442
Anti-mouse CD127, BV605 (A7R34)	Biolegend	Cat# 135041 RRID: AB_2572047
Anti-mouse KLRG1, PerCP-eFluor 710 (2F1)	eBioscience	Cat# 46-5893-80 RRID: AB_10671072
Anti-mouse Ly-6C, BV605 (HK1.4)	Biolegend	Cat# 128036 RRID: AB_2562353
Anti-mouse Ly-6G, PE-Cy7 (1A8)	BD Biosciences	Cat# 560601 RRID: AB_1727562
Anti-mouse Ly-6G, BV421 (1A8)	Biolegend	Cat# 127628 RRID: AB_2562567
Anti-mouse MHC-II, PE/Dazzle 594 (M5/114.15.2)	Biolegend	Cat# 107648 RRID: AB_2565979
Anti-mouse MHC-II, eFluor 450 (M5/114.15.2)	eBioscience	Cat# 48-5321-82 RRID: AB_1272204

(Continued on next page)

Continued

REAGENT or RESOURCE	SOURCE	IDENTIFIER
Anti-mouse NK1.1, eFluor 450 (PK136)	eBioscience	Cat# 48-5941-82 RRID: AB_2043877
Anti-mouse Sca-1, FITC (D7)	eBioscience	Cat# 11-5981-81 RRID: AB_465332
Anti-mouse TCR β , PerCP-Cy5.5 (H57-597)	eBioscience	Cat# 45-5961-82 RRID: AB_925763
Anti-mouse TCR $\gamma\delta$, eFluor 450 (eBioGL3)	eBioscience	Cat# 48-5711-82 RRID: AB_2574071
Anti-mouse TCR γ 3, FITC (536)	BD Biosciences	Cat# 553229 RRID: AB_394721
Anti-mouse IFN- γ , eFluor450 (XMG1.2)	eBioscience	Cat# 48-7311-82 RRID: AB_1834366
Anti-mouse IL-17A, AF488 (TC11-18H10.1)	Biolegend	Cat# 506910 RRID: AB_536012
Anti-mouse IL-17A, PE (eBio17B7)	eBioscience	Cat# 12-7177-81 RRID: AB_763582
Anti-mouse Ki-67, eFluor 450 (SolA15)	eBioscience	Cat# 48-5698-82 RRID: AB_11149124
Anti-mouse ROR γ t, PE (B2D)	eBioscience	Cat# 12-6981-82 RRID: AB_10807092
Anti-human/mouse T-bet, PE (eBio4B10)	eBioscience	Cat# 12-5825-82 RRID: AB_925761
Anti-human/mouse T-bet, APC (eBio4B10)	Biolegend	Cat# 644814 RRID: AB_10901173
Anti-human/mouse T-bet, BV421 (eBio4B10)	Biolegend	Cat# 644816 RRID: AB_10959653
Anti-human CD3 ϵ , PE (SP34-2)	BD Biosciences	Cat# 552127 RRID: AB_394342
Anti-human CD4, BV650 (L200)	BD Biosciences	Cat# 563737 RRID: AB_2687486
Anti-human CD8 α , APC-Cy7 (RPA-T8)	BD Biosciences	Cat# 557760 RRID: AB_396865
Anti-human CD45, BV421 (D058-1283)	BD Biosciences	Cat# 740084 RRID: N/A
Anti-human Granzyme B (GB11)	Molecular Probes	Cat# GRB04 RRID: AB_2536538
Anti-human IFN- γ , AF700 (B27)	BD Biosciences	Cat# 561024 RRID: AB_2033976
Anti-human IL-17A, AF488 (BL168)	Biolegend	Cat# 512307 RRID: AB_961387
Mouse V β TCR Screening Panel	BD Biosciences	Cat# 557004 RRID: AB_647180
CD11c Microbeads, mouse	Miltenyi Biotec	Cat #130-108-338 RRID: N/A
Keratin 14 Polyclonal Chicken Antibody, Purified	Biolegend	Cat #906001 RRID: AB_2565055
Goat Anti-Chicken IgG	Jackson ImmunoResearch Laboratories	Cat #103-605-155 RRID: AB_2337392

(Continued on next page)

Continued

REAGENT or RESOURCE	SOURCE	IDENTIFIER
Normal Goat Serum	Jackson ImmunoResearch Laboratories	Cat #005-000-121 RRID: AB_2336990
Rat Gamma Globulin	Jackson ImmunoResearch Laboratories	Cat #012-000-002 RRID: AB_2337135
Bacterial and Virus Strains		
<i>Staphylococcus epidermidis</i> NIH05001	Laboratory of Dr. Julie Segre (NHGRI/NIH)	N/A
<i>Staphylococcus epidermidis</i> NIHLM040	Laboratory of Dr. Julie Segre (NHGRI/NIH)	N/A
<i>Staphylococcus epidermidis</i> NIHLM061	Laboratory of Dr. Julie Segre (NHGRI/NIH)	N/A
<i>Staphylococcus epidermidis</i> NIHLM087	Laboratory of Dr. Julie Segre (NHGRI/NIH)	N/A
<i>Staphylococcus epidermidis</i> NIHLM088	Laboratory of Dr. Julie Segre (NHGRI/NIH)	N/A
<i>Staphylococcus epidermidis</i> NIHLM095	Laboratory of Dr. Julie Segre (NHGRI/NIH)	N/A
<i>Staphylococcus xylosus</i> 42C08	Laboratory of Dr. Julie Segre (NHGRI/NIH)	N/A
<i>Staphylococcus xylosus</i> 42G11	Laboratory of Dr. Julie Segre (NHGRI/NIH)	N/A
HSV-1 (F)	Laboratory of T.M.K.	N/A
Biological Samples		
Spleen from <i>Qa-1</i> ^{-/-} mice	Laboratory of Dr. Harvey Cantor (Harvard University)	Mouse strain: Jax 007907
Chemicals, Peptides, and Recombinant Proteins		
2-Mercaptoethanol (1,000X)	GIBCO	Cat # 21985-023
2-Mercaptoethanol	Sigma-Aldrich	Cat # M3148-25ML
BSA	Sigma-Aldrich	Cat# A3059-500G
Brefeldin A (GolgiPlug)	BD Biosciences	Cat# 555029
DAPI	Sigma-Aldrich	Cat # D9542
DMEM medium	Corning	Cat # 10-017-CV
DNase I	Sigma-Aldrich	Cat# DN25-5G
EDTA (0.5M)	Corning	Cat # 46-034-Cl
FBS	Hyclone	Cat # SH30070.03
L-Glutamine	Corning	Cat # 25-005-Cl
HEPES	Corning	Cat # 25-060-Cl
IMDM medium	Thermo Fisher Scientific	Cat # 12440079
Imiquimod (Aldara Crean 5%)	3M Health Care	N/A
Ionomycin	Sigma-Aldrich	Cat # I0634-5MG
Liberase TL	Roche	Cat# 05401020001
MEM Non-essential Amino Acids (100X)	Corning	Cat # 25-025-Cl
Paraformaldehyde	Electron Microscopy Sciences	Cat # 15714-S
Penicillin-Streptomycin (100X)	Corning	Cat # 30-002-Cl
Phorbol 12-myristate 13-acetate (PMA)	Sigma-Aldrich	Cat # P8139-10MG
ProLong Gold Antifade Mountant	Molecular Probes	Cat # P36930
Proteinase K	Invitrogen	Cat # 10005393
RNAlater	Sigma-Aldrich	Cat # R0901-100ML
RPMI 1640 medium	Corning	Cat # 10-040-CV
Sodium Pyruvate (100X)	Corning	Cat # 25-000-Cl
Triton X	Sigma-Aldrich	Cat #T9284
f-FMIVIL peptide (Fr38)	Genscript	N/A
f-MAYPFQLGL peptide (COII)	Genscript	N/A
f-MFFINIL peptide (ND1)	Genscript	N/A
f-MFILVN peptide	Genscript	N/A
f-MFINRW peptide (COI)	Genscript	N/A
f-MFLAWN peptide	Genscript	N/A

(Continued on next page)

Continued

REAGENT or RESOURCE	SOURCE	IDENTIFIER
f-MLKIIILPSL peptide (ND4)	Genscript	N/A
f-MFLLEL peptide	Genscript	N/A
f-MFLLVN peptide	Genscript	N/A
f-MFVVTN peptide	Genscript	N/A
f-MIFIYA peptide	Genscript	N/A
f-MIFVML peptide	Genscript	N/A
f-MIGWII peptide (LemA)	Genscript	N/A
f-MIIAII peptide	Genscript	N/A
f-MIIGYA peptide	Genscript	N/A
f-MIIINA peptide	Genscript	N/A
f-MILGLA peptide	Genscript	N/A
f-MILIID peptide	Genscript	N/A
f-MILLQL peptide	Genscript	N/A
f-MILMID peptide	Genscript	N/A
f-MILVQL peptide	Genscript	N/A
f-MIVLRR peptide	Genscript	N/A
f-MIYAGI peptide	Genscript	N/A
f-MIYAYI peptide	Genscript	N/A
f-MIYLDN peptide	Genscript	N/A
f-MIYLQN peptide	Genscript	N/A
f-MLFGRL peptide	Genscript	N/A
f-MLLFII peptide	Genscript	N/A
f-MLLFLC peptide	Genscript	N/A
f-MLLGSH peptide	Genscript	N/A
f-MLLIIA peptide	Genscript	N/A
f-MLLLAY peptide	Genscript	N/A
f-MLLPIQ peptide	Genscript	N/A
f-MLLPKR peptide	Genscript	N/A
f-MNENLFASF peptide (ATPase6)	Genscript	N/A
f-MNIFTTSIL peptide (ND5)	Genscript	N/A
f-MNLYTVIFI peptide (ND3)	Genscript	N/A
f-MNNYIFVLS peptide (ND6)	Genscript	N/A
f-MNPITLAI peptide (ND2)	Genscript	N/A
f-MPQLDTSTW peptide (ATPase8)	Genscript	N/A
f-MPSTFFNLT peptide (ND4L)	Genscript	N/A
f-MTHQTHAYH peptide (COIII)	Genscript	N/A
f-MTNMRKTHP peptide (Cytb)	Genscript	N/A
f-MYFVDK peptide	Genscript	N/A
f-MYYFVG peptide	Genscript	N/A
f-MIIINA:H2:M3-streptavidin-phycoerythrin	NIH Tetramer Core Facility	N/A
f-MIIINA:H2:M3-streptavidin-allophycocyanin	NIH Tetramer Core Facility	N/A
f-MIGWII:H2:M3-streptavidin-phycoerythrin	NIH Tetramer Core Facility	N/A
Critical Commercial Assays		
Arcturus PicoPure RNA Isolation kit	Thermo Fisher Scientific	Cat# KIT0204
BD Cytofix/Cytoperm	BD Biosciences	Cat# 554722
BD Perm/Wash	BD Biosciences	Cat# 554723
Foxp3 / Transcription Factor Staining Buffer Set	eBioscience	Cat# 00-5523-00
High Sensitivity D1000 ScreenTape	Agilent	Cat # 5067-5584

(Continued on next page)

Continued

REAGENT or RESOURCE	SOURCE	IDENTIFIER
LIVE/DEAD Fixable Blue Dead Cell Staining Kit	Life Technologies	Cat# L23105
MACS Cell Separation Column LS	Miltenyi Biotec	Cat #130-042-401
Nextera XT DNA Library Prep Kit	Illumina	Cat# FC-131-1096
NextSeq 500/550 v2 kits (75 cycles)	Illumina	Cat# FC-404-2005
QuantSeq 3' mRNA-Seq Library Prep Kit FWD for Illumina	Lexogen	Cat# 015.24
Qubit dsDNA HS Assay Kit	Molecular Probes	Cat # Q32854
RNeasy Fibrous Tissue Mini Kit	QIAGEN	Cat# 74704
SMARTer Ultra Low Input RNA Kit	Clonetech	Cat# 634946
Deposited data		
Raw RNA-Seq data	This paper	NCBI BioProject: PRJNA419368
Experimental Models: Organisms/Strains		
Mouse: C57BL/6	Taconic Farms	Mouse strain: C57BL/6NTac RRID: IMSR_TAC:b6
Mouse: B6.SJL-Cd45a(Ly5a)/Nai (B6.SJL)	NIAID-Taconic Exchange	Mouse strain: Tac 7
Mouse: B10.A-Cd45a(Ly5a)/Nai N5 (B10.A)	NIAID-Taconic Exchange	Mouse strain: Tac 31
Mouse: BALB/cJ	Jackson Laboratory	Mouse strain: Jax 000651 RRID: IMSR_JAX:000651
Mouse: FVB/NJ (FVB)	Jackson Laboratory	Mouse strain: Jax 001800 RRID: IMSR_JAX:001800
Mouse: SJL/JCrNTac (SJL)	Taconic Farms	Mouse strain: SJL RRID: IMSR_TAC:sjl
Mouse: C57BL/6-Tbet-ZsGreen[Tg] (T-bet-ZsGreen)	NIAID-Taconic Exchange	Mouse strain: Tac 8419
Mouse: B6.129-B2m ^{tm1Jae} N12 (B2m ^{-/-})	NIAID-Taconic Exchange	Mouse strain: Tac 253
Mouse: B6.129P2-H2-K1 ^{tm1Bpe} H2-D1 ^{tm1Bpe} /DcrJ (K ^b D ^{b-/-})	Jackson Laboratory	Mouse strain: Jax 019995 RRID: MSR_JAX:019995
Mouse: B6.129X1-Gt(ROSA) ^{26Gortm1(EYFP)Cos/J} (R26-stop-EYFP)	Jackson Laboratory	Mouse strain: Jax 006148 RRID: IMSR_JAX:006148
Mouse: B6.129S2-Tap1 ^{tm1Atp} /J (Tap1 ^{-/-})	Jackson Laboratory	Mouse strain: Jax 002944 RRID: IMSR_JAX:002944
Mouse: B6.129P2-Tcrd ^{tm1Mom} /J (TCRδ ^{-/-})	Jackson Laboratory	Mouse strain: Jax 002120 RRID: IMSR_JAX:002120
Mouse: B6.129-B2m ^{tm1Jae} N12 x B6-LY5.2/Cr	Laboratory of Rémy Bosselut (NCI/NIH)	N/A
Mouse: IL-17A-Cre	Laboratory of Dr. Brigitta Stockinger (The Francis Crick Institute)	Mouse strain: Jax 016879 RRID: IMSR_JAX:016879
Mouse: H2-M3 ^{-/-}	Laboratory of Chyung-Ru Wang (Northwestern University)	N/A
Mouse: germ-free C57BL/6	NIAID Microbiome Program Gnotobiotic Animal Facility	Mouse strain: C57BL/6NTac
Mouse: wild <i>Mus musculus domesticus</i>	Laboratory of B.R.	N/A
Non-human primate: <i>Macaca mulatta</i>	Laboratory of J.M.B.	N/A
<i>Leishmania major</i>	Laboratory of Dr. David Sacks (NIAID/NIH)	Friedlin (FV1)
Software and Algorithms		
DEseq2 package	Anders and Huber, 2010	RRID: SCR_000154
FastQC software package version 0.11.5	Babraham Bioinformatics	RRID: SCR_014583
Flowjo software	Treestar	RRID: SCR_008520
Imaris software	Bitplane	RRID: SCR_007370
multiqc	Ewels et al., 2016	

(Continued on next page)

Continued

REAGENT or RESOURCE	SOURCE	IDENTIFIER
Prism software	GraphPad	RRID: SCR_002798
RSEM package	Li and Dewey, 2011	RRID: SCR_013027
STAR aligner	Dobin et al., 2013	N/A
Trimmomatic	Bolger et al., 2014	RRID: SCR_011848

CONTACT FOR REAGENT AND RESOURCE SHARING

Further information and requests for resources and reagents should be directed to and will be fulfilled by the Lead Contact, Yasmine Belkaid (ybelkaid@niaid.nih.gov).

EXPERIMENTAL MODEL AND SUBJECT DETAILS**Mice**

C57BL/6NTac and SJL/JCrNTac (SJL) specific pathogen-free mice were purchased from Taconic Farms. Germ-free C57BL/6 mice were bred and maintained in the NIAID Microbiome Program gnotobiotic animal facility. B6.SJL (B6.SJL-Cd45a(Ly5a)/Nai), B10.A (B10.A-Cd45a(Ly5a)/NAi N5), T-bet-ZsGreen (C57BL/6-Tbet-ZsGreen[Tg]), and *B2m*^{-/-} (B6.129-*B2m*^{tm1Jae} N12) mice were obtained through the NIAID-Taconic exchange program. BALB/c, FVB, *K^bD^b*^{-/-} (B6.129P2-H2-*Kb*^{tm1} H2-*Db*^{tm1} N12), R26-stop-EYFP (B6.129X1-Gt(ROSA)^{26Sor tm1(EYFP)Cos}/J), *Tap1*^{-/-} (B6.129S2-*Tap1*^{tm1Atp}/J) and *TCR^{-/-} (B6.129P2-*Tcrd*^{tm1Mon}/J) mice were purchase from the Jackson Laboratory. IL-17A-Cre mice were kindly provided by Dr. B. Stockinger (The Francis Crick Institute). *H2-M3*^{-/-} mice were kindly provided by Dr. C. Wang (Northwestern University) and bred in house with WT C57BL/6. *Qa-1*^{-/-} mouse spleens were kindly provided by Dr. H Cantor (Harvard University). Congenic *β2 m*^{-/-} (B6.129-*B2m*^{tm1Jae} N12 x B6-LY5.2/Cr) were kindly provided by Dr. R. Bosselut (National Cancer Institute, NIH). All mice were bred and maintained under specific pathogen-free conditions at an American Association for the Accreditation of Laboratory Animal Care (AAALAC)-accredited animal facility at the NIAID and housed in accordance with the procedures outlined in the Guide for the Care and Use of Laboratory Animals. All experiments were performed at the NIAID under an animal study proposal (LPD11E) approved by the NIAID Animal Care and Use Committee. Sex and age-matched mice between 6 and 12 weeks of age were used for each experiment. Wild *Mus musculus domesticus* were trapped in Maryland. Trapping was carried out in concordance with local laws and was carried out with the approval of the relevant regulatory bodies under protocol approved by the NIDDK Animal Care and Use Committee.*

Non-human primates

Non-human primates were housed at the NIH animal center. All procedures were carried out under ketamine anesthesia by trained personnel under the supervision of veterinary staff and all efforts were made to ameliorate the welfare and to minimize animal suffering in accordance with the “Weatherall report for the use of non-human primates” recommendations under animal protocol LPD26. Animals were housed in adjoining individual primate cages allowing social interactions, under controlled conditions of humidity, temperature and light (12-hour light/12-hour dark cycles). Food and water were available *ad libitum*. Animals were monitored twice daily and fed commercial monkey chow, treats and fruit twice daily by trained personnel. The study included 3 adult rhesus macaques (2 males and 1 female). All monkeys were housed and cared for in accordance with AAALAC standards in AAALAC-accredited facilities, and all animal procedures performed according to protocols approved by the NIAID Animal Care and Use Committee.

METHODS DETAILS**Topical association and intradermal infection of mice with *Staphylococcus* species**

S. epidermidis strains (NIHLM040, NIHLM095, NIHLM061, NIHLM088, NIH05001, and NIHLM087) and *S. xylosus* strains (42C08 and 42G11) were cultured for 18 hours in tryptic soy broth at 37°C. For topical association of bacteria, each mouse was associated by placing 5 mL of the bacterial suspension (approximately 10⁹ CFU/ml) across the entire skin surface (approximately 36 cm²) using a sterile cotton swab. Application of bacterial suspension was repeated every other day a total of four times. In experiments involving topical application of various bacterial species or strains, 18-hour cultures were normalized using OD₆₀₀ to achieve similar bacterial density (approximately 10⁹ CFU/ml). For some experiments, mice were infected intradermally in the ear pinnae with 10⁷ c.f.u. of *S. epidermidis* strain NIHLM087.

***Leishmania major* and herpes simplex virus type 1 (HSV-1) skin infections**

C57BL/6 mice were infected intradermally in the ear pinnae with *L. major* (5x10³ metacyclic promastigotes) using a 29 gauge needle in a 10 µL volume. For HSV infection, C57BL/6 mice were anaesthetized with isoflurane and areas of the flank were depilated with Nair. The next day mice were anaesthetized with Avertin and a 2 cm² area of the flank was abraded for 5 s with a Dremel 4000 variable

speed tool (setting 10) containing a 1-cm width medium grit sanding bit. 1×10^6 plaque forming units (PFU) of HSV-1 (F) in DMEM containing 10% FBS was applied and gently rubbed into the abraded area with a pipette tip. Mice were maintained with the flank exposed until recovery. Mice that received a productive skin infection were sacrificed 14 days later and flanks were processed for cell sorting.

Imiquimod induced psoriasis-like dermatitis

Mice between 6 and 8 weeks of age were treated daily for 7 days on ear pinnae with 10 mg of 5% Imiquimod (IMQ) cream (Aldara Cream 5%; 3M Health Care, UK) (adapted from [van der Fits et al. \[2009\]](#)).

Non-human primate skin and association with *S. epidermidis*

For characterization of CD8⁺ T cells at steady state, non-human primate skin tissue was obtained from the glabella of 4 healthy rhesus macaques (*Macaca mulatta*). For association with *S. epidermidis*: rhesus macaques (RM) were anesthetized with ketamine and a 5-cm x 5-cm area of each dorsal forearm and each side of upper back was shaved with a hair clipper (4 sites total per RM). As a control, two 6-mm biopsies were taken from forearm and upper back of one side of each RM for T cell analysis prior to *S. epidermidis* association. This was done to prevent contamination of the control site with bacteria. Next, contralateral forearm and upper back sites were topically associated with a culture of *S. epidermidis* soaked onto a 5-cm x 5-cm piece of gauze dressing and taped to the site for one hour prior to removal. Topical application was repeated every other day for a total of 4 applications. Fourteen days later two 6-mm punch biopsies were taken from each contralateral site and analyzed for T cell responses. Values from the two biopsies from each site were averaged when computing frequencies and total numbers of T cells.

***S. epidermidis* conditioned medium preparation**

NIHLM087 was cultured for 24 hours in IMDM (Invitrogen) supplemented with 2 mM L-glutamine, 1 mM sodium pyruvate and nonessential amino acids, 20 mM HEPES with shaking at 37°C. Bacterial culture was centrifuged at 3200 g for 30 minutes. Supernatant was then filtered through 0.22 µm filter (Millipore). For experiments that involved Proteinase K digestion (Sigma), 5×10^9 cfu heat-killed NIHLM087 in PBS or 1mL of NIHLM087 conditioned medium was incubated with β-mercaptoethanol (1mM final concentration, Sigma) and 300 µg Proteinase K. The solutions were incubated for 24 hours at 56°C followed by a 95°C, 30 minutes denaturation step.

Tissue processing

Murine tissues

Cells from lymph nodes and spleen were mashed through a 70-micron cell strainer to generate single cell suspensions. Ears were excised and separated into ventral and dorsal sheets. Flank (dorsal) skin was shaved with chrom mini (Wahl), subcutaneous fat tissue was removed with a number 10 scalpel, and skin was cut into 1cm by 1cm pieces. Ear pinnae and flank tissues were digested in digestion media (RPMI 1640 media supplemented with 2 mM L-glutamine, 1 mM sodium pyruvate and nonessential amino acids, 55 µM β-mercaptoethanol, 20 mM HEPES, 100 U/ml penicillin, 100 µg/ml streptomycin and 0.25 mg/ml Liberase TL purified enzyme blend, Roche), and incubated for 2 hours at 37°C and 5% CO₂. Digested skin sheets were homogenized using the Medicon/Medimachine tissue homogenizer system (Becton Dickinson).

Non-human primate skin

Subcutaneous fat tissue was scraped off with a number 10 scalpel blade. Skin tissue was then weighted and perfused with 100-500 µL of digestion media (RPMI 1640 media supplemented with 2 mM L-glutamine, 1 mM sodium pyruvate and nonessential amino acids, 20 mM HEPES, 100 U/ml penicillin, 100 µg/ml streptomycin and 0.25 mg/ml Liberase TL purified enzyme blend, Roche). Perfused skin tissue was placed in 5 mL of digestion media dermal side down and incubated for 1 hour at 4°C. Tissue was then minced with scissors in 5 mL of fresh digestion media and incubated at 37°C, 5% CO₂ with shaking. After 1 hour, digestion was stopped by adding 100 µL of 0.5 M EDTA and 1 mL of fetal bovine serum. Digested tissue was then mashed through a 70-micron cell strainer to obtain a single cell suspension.

Wounding study

C57BL/6 mice in the telogen phase of the hair cycle were anaesthetized and given punch biopsies on the ear or back. For ear wounds, a 2.5mm diameter corneal trephine blade (Ambler Surgical) was used to punch a through and through wound (hole) in the center of each ear. Tissue was collected at 3d after wounding for microscopy. For backskin wounds, dorsal hairs were cut with a clipper and a 6mm biopsy punch was used to partially perforate skin. An iris scissors was then used to cut epidermis and dermis along outline to create a full thickness wound in the shape of a circle.

Immunofluorescence/confocal microscopy of ear pinnae

Ear pinnae were split with forceps, fixed in 1% paraformaldehyde solution (Electron Microscopy Sciences) overnight at 4°C and blocked in 1% BSA, 0.25% Triton X blocking buffer for 2 hours at room temperature. Tissues were first stained with anti-CD8α (clone 53-6.7, eBioscience), anti-Sca-1 (D7, eBioscience) and/or rabbit anti-CD31 (390, eBioscience), and anti-Ki67 (solA15, eBioscience) antibodies overnight at 4°C, washed three time with PBS and then stained with 4', 6-diamidino-2-phenylindole (DAPI, Sigma-Aldrich) for 5 min at room temperature and before being mounted with ProLong Gold (Molecular Probes) antifade reagent. Ear pinnae images

were captured on a Leica TCS SP8 confocal microscope with a 40X oil objective (HC PL APO 40X/1.3 oil). Images were analyzed using Imaris Bitplane software.

Immunofluorescence/epifluorescence microscopy of backskin wounds

Wounded backskin tissue was incubated in 30% sucrose at 4°C overnight, fixed in 4% paraformaldehyde, embedded in OCT compound (Tissue-Tek), frozen on dry ice, and cryo-sectioned (20 µm section thickness). Sections were fixed in 4% paraformaldehyde, rinsed with PBS, permeabilized 10 min with 0.1% Triton X-100 (Sigma) in PBS, then blocked for 1 hour in blocking buffer (2.5% normal goat serum (Jackson ImmunoResearch), 1% BSA, 0.3% Triton X-100). Primary antibody to K14 (chicken, 1:400, Biolegend) was used. Primary antibody was diluted in blocking buffer with Rat gamma globulin (Jackson ImmunoResearch) and anti-CD16/32 (ebioscience) and incubated at 4°C overnight. After washing with PBS, a secondary antibody, conjugated with Alexa647 (goat, Jackson ImmunoResearch) was added for 2 hours at room temperature. Slides were washed with PBS, counterstained with DAPI and mounted in Prolong Gold. Wound images were captured with a Leica DMI 6000 widefield epifluorescence microscope equipped with a Leica DFC360X monochrome camera. Tiled and stitched images of wounds were collected using a 20X/0.4NA dry objective. Images were analyzed using Imaris Bitplane software.

In vitro re-stimulation

For detection of basal cytokine potential, single cell suspensions from various tissues were cultured directly ex vivo in a 96-well U-bottom plate in complete medium (cRPMI-RPMI 1640 supplemented with 10% fetal bovine serum [FBS], 2 mM L-glutamine, 1 mM sodium pyruvate and nonessential amino acids, 20 mM HEPES, 100 U/ml penicillin, 100 µg/ml streptomycin, 50 mM β-mercaptoethanol) and stimulated with 50 ng/ml phorbol myristate acetate (PMA) (Sigma-Aldrich) and 5 µg/ml (mouse) or 1 µg/ml (non-human primate) ionomycin (Sigma-Aldrich) in the presence of brefeldin A (GolgiPlug, BD Biosciences) for 2.5 hours at 37°C in 5% CO₂. After stimulation, cells were assessed for intracellular cytokine production as described below.

Phenotypic analysis

Murine single cell suspensions were incubated with fluorochrome-conjugated antibodies against surface markers: CCR6 (29-2L17), CD3ε (145-2C11), CD4 (clone RM4-5), CD8β (eBioH35-17.2), CD11b (M1/70), CD11c (N418), CD19 (6D5), CD24 (M1/69), CD44 (IM7), CD45 (30-F11), CD45.1 (A20), CD45.2 (104), CD64 (X54-5/7.1), CD69 (H1.2F3), CD103 (2E7), CD122 (TM-b1), CD127 (A7R34), KLRG1 (2F1), Ly-6C (HK1.4), Ly-6G (1A8), MHCII (M5/114.15.2), TCRβ (H57-597), TCRγ3⁺ (536), and mouse Vβ screening panel (Becton Dickinson) in Hank's buffered salt solution (HBSS) for 20 min at 4°C and then washed. LIVE/DEAD Fixable Blue Dead Cell Stain Kit (Invitrogen Life Technologies) was used to exclude dead cells. Cells were then fixed for 20 min at 4°C using BD Cytofix/Cytoperm (Becton Dickinson) and washed twice. For intracellular cytokine staining, cells were stained with fluorochrome-conjugated antibodies against IFN-γ (XMG-1.2), IL-17A (eBio17B7), and/or Granzyme B (human, GB11) in BD Perm/Wash Buffer (Becton Dickinson) for 45 min at 4°C. For transcription factor staining, cells were fixed and permeabilized with the FoxP3/Transcription Factor staining buffer set (eBioscience) and stained with fluorochrome-conjugated antibodies against T-bet (ebio4B10) or RORγt (B2D) for 45 min at 4°C. Each staining was performed in the presence of purified anti-mouse CD16/32 (2.4G2), 0.2 mg/ml purified rat gamma globulin (Jackson ImmunoResearch). Staining of cells from non-human primate skin tissue was performed using a similar protocol and the following antibodies against human proteins: CD3ε (SP34-2), CD4 (L200), CD8α (RPA-T8), CD45 (D058-1283), IFN-γ (B27) and IL-17A (BL168). All antibodies were purchased from eBioscience, Biolegend, BD Biosciences, or Miltenyi Biotec. Cell acquisition was performed on an LSRII flow cytometer using FACSDiVa software (BD Biosciences) and data were analyzed using FlowJo software (TreeStar).

In vivo recall of f-MIIINA:H2-M3-specific CD8⁺ T cells via intravenous peptide injection

Cytokine production was elicited by i.v. injection of 100 µg of f-MIIINA peptide in PBS via the tail vein of mice that were previously topically associated with *S. epidermidis* strain NIHLM087. Mice were euthanized after 3 hours, and single-cell suspensions were made from pooled skin draining lymph nodes and spleen or ear pinnae in cRPMI medium supplemented with brefeldin A (10 µg/ml; Sigma). Cytokine production by f-MIIINA:H2-M3-specific CD8⁺ T cells from mice injected with f-MIIINA peptide was determined before (ear pinnae) or after tetramer-based cell enrichment (spleen and lymph nodes) as described below.

Cell enrichment

Spleen and lymph node cells were prepared and stained for 1 hour at room temperature with f-MIIINA:H2-M3-streptavidin-phycerythrin, f-MIIINA:H2-M3-streptavidin-allophycocyanin, and/or f-MIGWII:H2-M3-streptavidin-allophycocyanin tetramers. Samples were then enriched for bead-bound cells on magnetized columns, and a portion was removed for counting. The rest of the sample underwent surface staining on ice with a mixture of antibodies described above.

DC-T cell co-culture assay

CD45⁺ CD90.2⁺ CD8β⁺ T cells (> 95% purity) were FACsorted from the ear skin tissue of C57BL/6 mice two weeks after topical association with *S. epidermidis* strain NIHLM087 using a FACSaria cell sorter. For splenic DC purification, single-cell suspensions from the spleen of congenic wild-type, *B2m*^{-/-}, *K^bD^b*^{-/-}, *Qa-1*^{-/-}, or *H2-M3*^{-/-} mice were magnetically enriched for CD11c⁺ cells by positive selection using CD11c MicroBeads and MACS separation columns (Miltenyi Biotec). Purified splenic dendritic cells

(SpDC) and CD8 β^+ T cells were co-cultured at a 15:1 ratio (5x10³ CD8 β^+ T cells) in a 96-well U-bottom plate in complete medium for 16 hours at 37°C in 5% CO₂. Brefeldin A (GolgiPlug) was added for the final 4 hours of culture. SpDC were previously incubated for 2 hours with or without heat-killed *S. epidermidis* (bacteria:SpDC ratio, 500:1) and washed before co-culture with CD8 β^+ T cells. For samples in which *S. epidermidis* conditioned medium (CM) was added, 40 μ L of CM was added directly to co-cultured cells and incubated for 16 hours. For samples in which fMet peptides were added, peptides were added at a final concentration of 15 μ g/ml. CD8 β^+ T cell cytokine production following co-culture was assessed by flow cytometry after surface and intracellular cytokine staining using the following antibodies: CD4, CD8 β , CD45.1, CD45.2, TCR- β , IFN- γ and IL-17A.

T cell isolation and RNA extraction for RNA-sequencing

T cells were FACsorted from the skin draining lymph nodes, ear or flank skin tissue of C57BL/6 mice. T cells were isolated from naive mice or those topically-associated with *S. epidermidis* NIHLM087, infected via intradermal route with *S. epidermidis* NIHLM087, or *Leishmania major*, topically administered with Imiquimod, or infected with Herpes Simplex Virus via skin scarification. Groups included: T_{EM} (lymph nodes; CD45 $^+$ CD90.2 $^+$ TCR β^+ CD8 β^+ CD44^{high} CD62L^{low}), Tc17 (skin; Lineage $^-$ CD45 $^+$ CD90.2 $^+$ TCR $\gamma\delta^-$ TCR β^+ CD8 β^+ CCR6 $^+$), Tc1 (skin; Lineage $^-$ CD45 $^+$ CD90.2 $^+$ TCR $\gamma\delta^-$ TCR β^+ CD8 β^+ CCR6 $^+$), DETC (skin; Lineage $^-$ CD45 $^+$ CD90.2 $^+$ TCR $\gamma\delta^+$ TCR β^- CD4 $^+$ CD8 β^-). The lineage cocktail consisted of antibodies to CD11b, CD11c, MHC-II, NK1.1, CD49f and CD19. RNA was extracted from T cell populations using the Arcturus PicoPure RNA Isolation Kit (Applied Biosystems), as per manufacturer's instructions.

RNA library preparation and sequencing

mRNA libraries were constructed using SMARTer Ultra Low Input RNA kit (Clonetech) + Nextera XT DNA library prep kit (Illumina). mRNA samples were pooled and sequenced on 3 lanes of HiSeq40000 with Illumina Hiseq3000/4000 chemistry. The reads from the Illumina Hi-seq sequencer in fastq format were verified for quality control using fastqc software package. The low-quality segments of the read along with adaptors were trimmed with the tool Trimmomatic (Ewels et al., 2016). The quality filtered reads were aligned to mouse genome GRCM38 using RSEM package (Li and Dewey, 2011) with default parameters and STAR aligner (Dobin et al., 2013). The expected RSEM counts were rounded to the nearest integer value and the transcripts with zero counts across all the samples are filtered out. T cell populations were compared using DESeq2 package (Anders and Huber, 2010).

Whole tissue RNA-sequencing and transcriptome analysis

A ~1mm skin region surrounding the wound site of backskin wounds was micro-dissected at each time point after initial wounding described above and submerged in RNAlater (Sigma) and stored at -20°C. Total tissue RNA was isolated from skin tissue using the RNeasy Fibrous Tissue Mini Kit (QIAGEN), as per manufacturer's instructions. A 3'end mRNA sequencing library was prepared using 100ng of total input RNA with the QuantSeq 3' mRNA-Seq Library Prep Kit FWD for Illumina (Lexogen) as per manufacturer's instructions. Libraries were quantified using an Agilent Tapestation (High Sensitivity D1000 ScreenTape) and Qubit (Thermo Fisher Scientific). Libraries (n = 24) were then pooled at equimolar concentrations and sequenced on an Illumina Nextseq 500 using the High Output v2 kit (75 cycles). Resultant data was demultiplexed on Illumina Basespace server using blc2fastq tool. The reads from the Illumina Next-seq sequencer in fastq format were verified for quality control using FastQC software package and summarized using multi-qc (Ewels et al., 2016). The low-quality segments of the read are trimmed with the tool Trimmomatic (Bolger et al., 2014) using: seed mismatches:3, palindrome clip threshold:50, simple clip threshold:10, sliding window:4, required quality:20, minimum length after trimming: 40 and maximum read length to error rate of 50:0.8. The quality filtered reads are aligned to mouse genome GRCM38 using RSEM package (Li and Dewey, 2011) with default parameters and STAR aligner (Dobin et al., 2013). The expected RSEM counts are rounded to the nearest integer value and the transcripts with zero counts across all the samples are filtered out. Differential expression analysis was performed using DESeq package (Anders and Huber, 2010) between two cohorts of mice (WT and H2-M3 $^{-/-}$) at different time points after wounding.

QUANTIFICATION AND STATISTICAL ANALYSIS

Statistical analysis

Groups were compared with Prism software (GraphPad) using the two-tailed unpaired or paired Student's t test. Flow cytometry plots are presented as mean \pm standard deviation. All other data are presented as mean only or mean \pm standard error of the mean. p < 0.05 was considered significant unless otherwise stated. Principle component analysis and accompanying confidence intervals of RNA-seq data were performed using a custom script combining functions in the R packages 'stats', 'vegan', and 'ggplot2'. The R package 'Vennable' was used to compute the Venn diagram shown.

DATA AND SOFTWARE AVAILABILITY

The accession number for the RNA-Seq datasets reported in this paper is NCBI BioProject: PRJNA419368.

Supplemental Figures

Cell

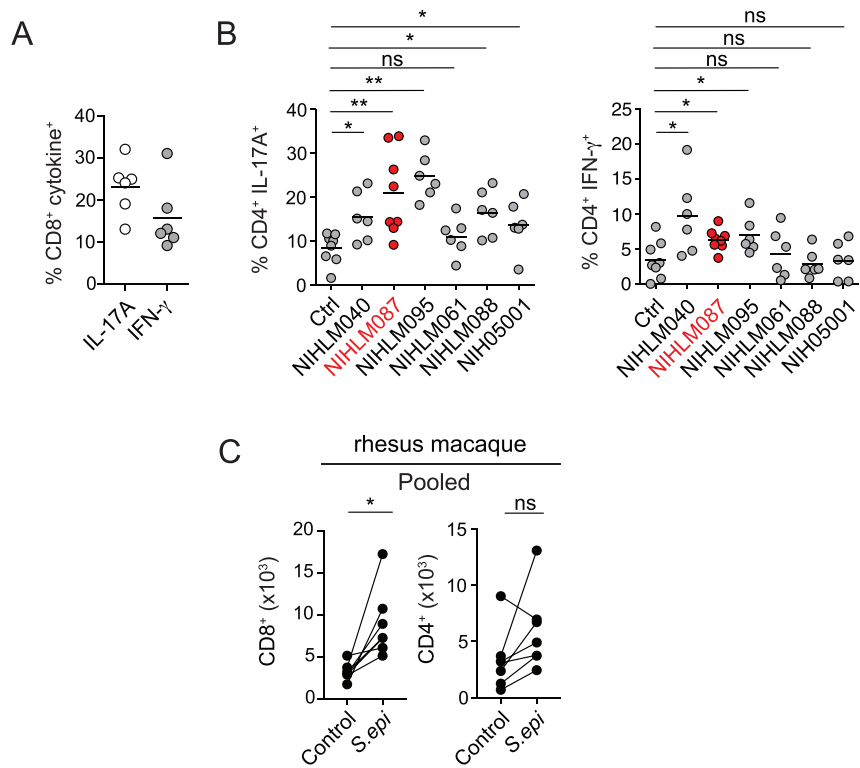


Figure S1. Most *S. epidermidis* Isolates Promote the Accumulation of CD4⁺ Effector T Cells to Skin, Related to Figure 1

(A) Frequencies of IL-17A⁺ or IFN- γ ⁺ CD8⁺ T cells isolated from rhesus macaque. All cells were isolated from glabella.

(B) Frequencies of IL-17A⁺ and IFN- γ ⁺ CD4⁺ T cells in control mice or mice topically associated with the indicated *S. epidermidis* isolate. All cells were isolated from ear pinnae. Student's t test was used to measure significance. * p < 0.05, ** p < 0.005.

(C) Number of CD8⁺ or CD4⁺ T cells in unassociated (control) or two weeks post *S. epidermidis* (NIHLM087) association (contralateral side) isolated from rhesus macaque. All cells were isolated from dorsal forearm or upper back. Paired points denote same animal.

(A and B) Each dot represents an individual animal.

(A-C) Cells were stimulated with PMA and ionomycin. Data are representative of 2-3 independent experiments.

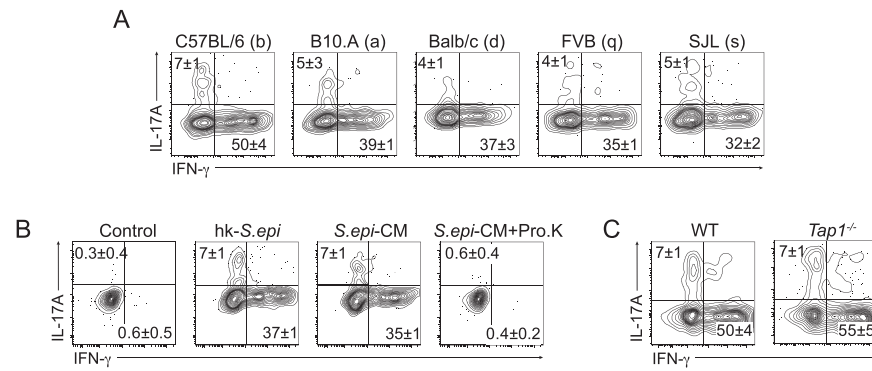


Figure S2. MHC I^{b} Restriction and Specificity Requirements of Commensal-Specific CD8 $^{+}$ T Cells in Skin, Related to Figure 2

(A–C) *In vitro* recall of commensal induced CD8 $^{+}$ T cells from skin with (A and C) heat-killed *S. epidermidis* or (B) heat-killed *S. epidermidis* and *S. epidermidis* conditioned medium (CM) loaded splenic DCs. Frequencies of IL-17A $^{+}$ or IFN- γ $^{+}$ CD8 $^{+}$ T cells after overnight culture. Splenic dendritic cells were enriched from wild-type C57BL/6 (WT), B10.A, BALB/c, FVB, SJL, or *Tap1*^{-/-} mice. Control = unloaded splenic dendritic cells (A) Haplotypes of strains shown in parentheses. All cells were isolated from ear pinnae of *S. epidermidis* associated mice 2 weeks after application. Plots are gated on live CD45 $^{+}$ TCR β $^{+}$ CD8 $^{+}$ T cells. Numbers in flow cytometry plots correspond to the frequencies of gated populations \pm SD.

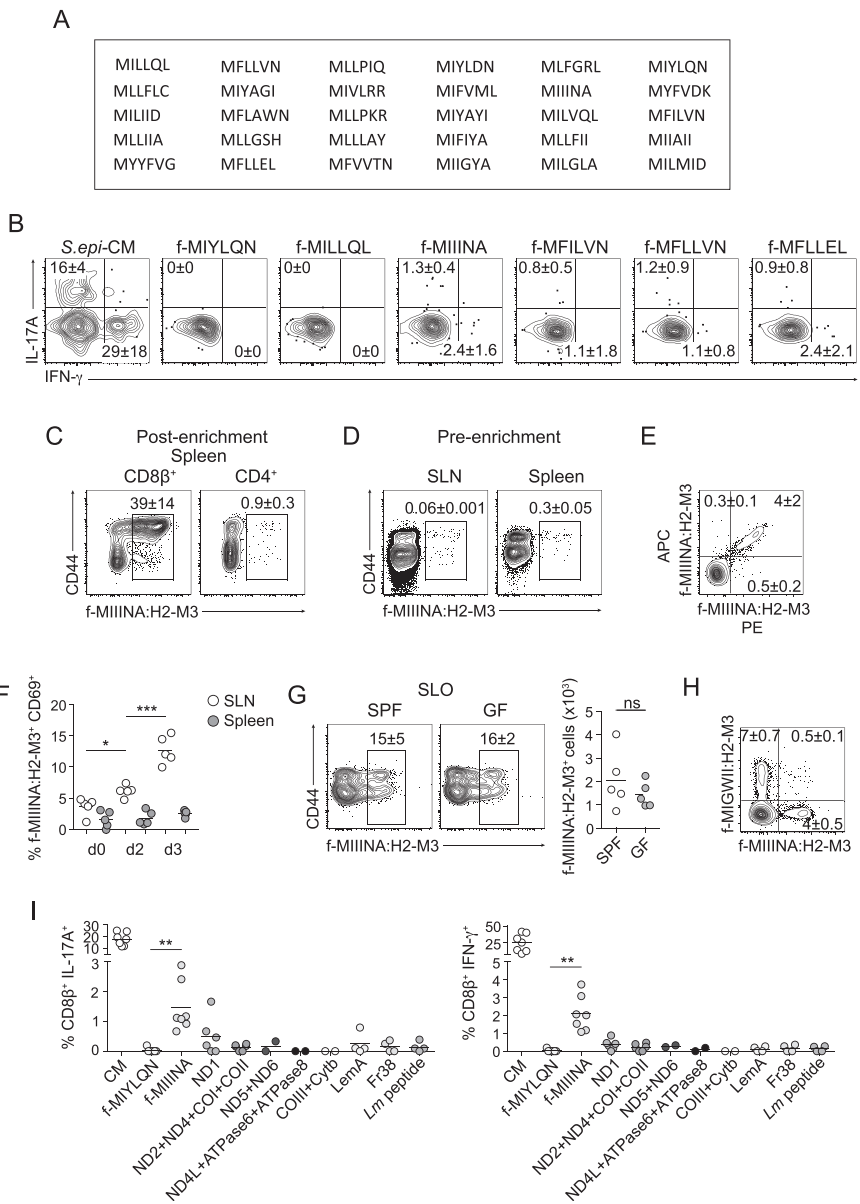


Figure S3. H2-M3-Restricted CD8⁺ T Cells Are Specific to *S. epidermidis*-Derived fMet Peptide Ligands, Related to Figure 3

(A) Panel of 30 fMet containing peptides tested that fit H2-M3 binding motif described by Chun et al. *JEM* 2001.

(B) *In vitro* recall of commensal induced CD8⁺ T cells from FACsorted skin with *S. epidermidis* conditioned medium (CM) or formyl peptide loaded splenic DCs. Frequencies of IL-17A⁺ or IFN-γ⁺ CD8⁺ T cells after overnight culture. Plots are gated on live CD45⁺ TCRβ⁺ CD8⁺ T cells. Splenic dendritic cells were enriched from wild-type mice. Numbers in flow cytometry plots correspond to the frequencies of gated populations ± SD.

(C and D) Frequencies of f-MIIIINA:H2-M3 tetramer positive cells. Gated on CD8^{β+} or CD4⁺ T cells in intact WT mice after (C) or before (D) magnetic bead enrichment. All cells were isolated from skin draining lymph nodes (SLN) or spleen of *S. epidermidis* associated mice one or two weeks after application. Plots are gated on live CD45⁺ Lineage (MHCII, CD11b, γδTCR)⁻ CD90.2⁺ CD3ε⁺ CD8^{β+} T cells. Numbers in flow cytometry plots correspond to the frequencies of gated populations ± SD.

(E) Frequencies of f-MIIIINA:H2-M3-APC, f-MIIIINA:H2-M3-PE single and double tetramer positive cells. All cells were isolated from pooled skin draining lymph nodes and spleen of naive SPF mice. Plot is gated on live CD45⁺ Lineage (MHCII, CD11b, γδTCR) CD90.2⁺ CD3ε⁺ CD8^{β+} T cells. Numbers in flow cytometry plots correspond to the frequencies of gated populations ± SD.

(F) Frequencies of f-MIIIINA:H2-M3 tetramer positive CD69⁺ cells in SLN or spleen in naive mice or mice that were previously *S. epidermidis* associated 2 or 3 days prior. Gated on live CD45⁺ Lineage (MHCII, CD11b, γδTCR) CD90.2⁺ CD3ε⁺ CD8^{β+} T cells.

(G) Frequencies and numbers of f-MIIIINA:H2-M3 tetramer positive cells in SLO of naive (non-S.epi associated) SPF or germ-free mice. Plots are gated on live CD45⁺ Lineage (MHCII, CD11b, γδTCR) CD90.2⁺ CD3ε⁺ T cells. Numbers in flow cytometry plots correspond to the frequencies of gated populations ± SD.

(legend continued on next page)

(H) Frequencies of f-MIGWII:H2-M3-APC or f-MIIINA:H2-M3-PE tetramer positive cells. All cells were isolated from pooled skin draining lymph nodes and spleen of naive SPF mice. Plot is gated on live CD45⁺ Lineage (MHCII, CD11b, $\gamma\delta$ TCR)⁻ CD90.2⁺ CD3ε⁺ CD8β⁺ T cells. Numbers in flow cytometry plots correspond to the frequencies of gated populations \pm SD.

(I) *In vitro* recall of commensal induced CD8⁺ T cells from FACsorted skin with *S. epidermidis* conditioned medium (CM), mitochondrial formyl peptides (ND1, ND2, ND4, ND4L, ND5, ND6, COI, COII, COIII, Cytb, ATPase6, ATPase8), or *Listeria monocytogenes*-derived formyl peptides (LemA [MIGWII], Fr38, *Lm* peptide) loaded splenic DCs. Frequencies of IL-17A⁺ or IFN-γ⁺ CD8β⁺ T cells after overnight culture. Plots are gated on live CD45⁺ TCRβ⁺ CD8β⁺ T cells. Splenic dendritic cells were enriched from wild-type mice.

(C and E-H) Magnetic bead enrichment was used to isolate all tetramer⁺ cells from SLO. Data are representative of 2-3 independent experiments.

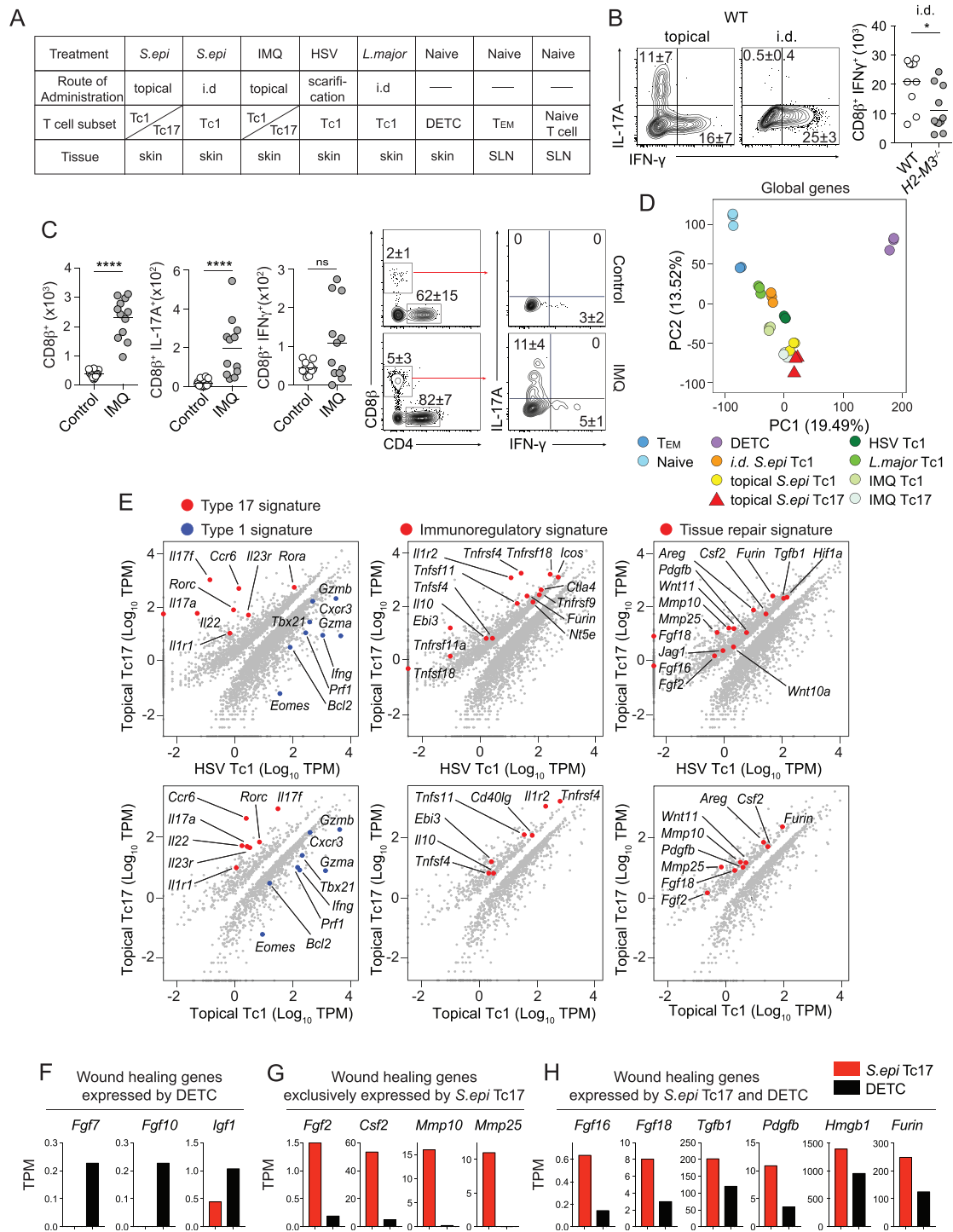


Figure S4. Commensal-Specific Tc17 Cells Express Transcripts Associated with Tissue Repair, Related to Figure 4

(A) T cell populations FACS sorted for RNA-sequencing analysis.

(B) Frequencies and numbers of IL-17A⁺, or IFN-γ⁺ CD8β⁺ T cells in WT or H2-M3^{-/-} mice one week post topical association or intradermal (i.d.) infection with *S. epidermidis* (NIHLM087). All cells were isolated from ear pinnae. Plots are gated on live CD45⁺ TCRβ⁺ CD8β⁺ T cells. Numbers in flow cytometry plots correspond to the frequencies of gated populations ± SD. Each dot in graph represents an individual mouse.

(C) Numbers and frequencies of total, IL-17A⁺, or IFN-γ⁺ CD8β⁺ T cells in untreated (control) or Imiquimod treated (IMQ) WT mice. All cells were isolated from ear pinnae. Plots are gated on live CD45⁺ TCRβ⁺ CD8β⁺ T cells. Numbers in flow cytometry plots correspond to the frequencies of gated populations ± SD. Each dot in graph represents an individual mouse.

(legend continued on next page)

-
- (D) Principle component analysis of global gene expression from FACsorted populations identified in (Figure S4A).
- (E) Diagonal plots showing differentially expressed genes (> 2-fold, $P_{adj} < 0.05$) comparing topical *S. epidermidis* specific Tc17 to HSV specific Tc1 cells in skin or topical *S. epidermidis* specific Tc1.
- (F–H) Gene expression measured in transcripts per million (TPM) comparing topical *S. epidermidis*-induced Tc17 to DETC.
- (B and C) Student's t test was used to measure significance. * $p < 0.05$, *** $p < 0.0001$.

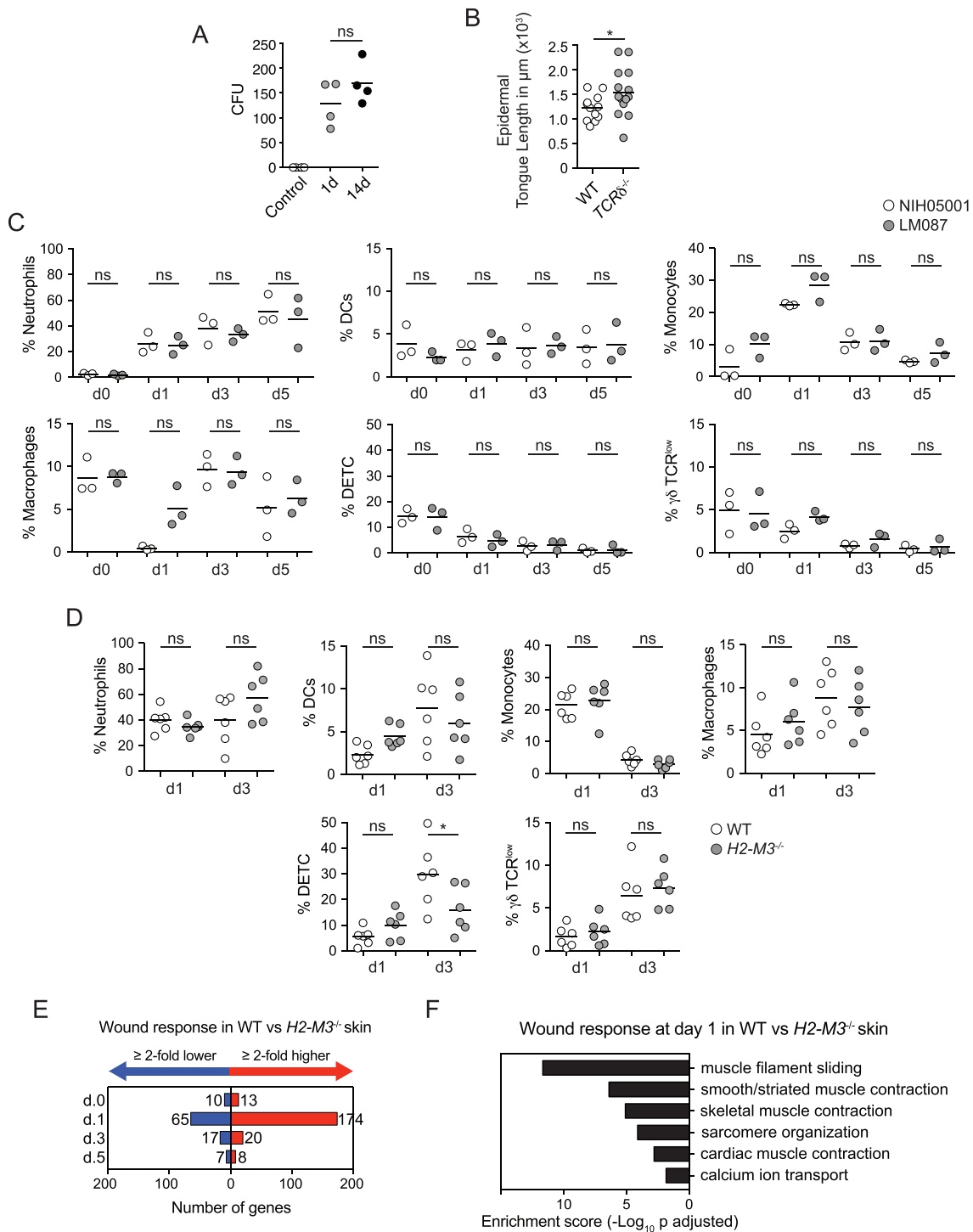


Figure S5. Commensal-Specific CD8⁺ T Cells Accelerate Wound Healing, Related to Figure 5

- (A) Enumeration of colony-forming units (cfu) from the ears after *S. epidermidis* topical association. Control = not associated with bacteria. Each dot represents cfu measurement from two ears of an individual mouse.
- (B) Quantification of the length of the tongue of epidermal keratinocytes that migrate in from the wound edges during re-epithelialization of the wound bed in WT or $TCR\delta^{-/-}$ mice. Mice were topically skin associated with NIHLM087. Tongue lengths were measured at 5 days after backskin punch biopsy.
- (C) Frequencies (of total CD45⁺ cells) of neutrophils, dendritic cells, monocytes, macrophages, DETC, and dermal $\gamma\delta$ T cells in the skin of WT mice 0–5 days after back skin punch biopsy of mice previously topically skin associated with either NIH05001 or LM087 *S. epidermidis* strains. Student's t test was used to measure significance.

(legend continued on next page)

-
- (D) Frequencies (of total CD45⁺ cells) of neutrophils, dendritic cells, monocytes, macrophages, DETC, and dermal $\gamma\delta$ T cells in the skin of WT or *H2-M3*^{-/-} mice 1 or 3 days after back skin punch biopsy of mice previously topically skin associated with *S. epidermidis* strain NIHLM087.
- (E) Whole skin tissue RNA-sequencing gene expression analysis. Numbers of genes with a >2 fold increase (red) or decrease (blue) in expression levels between the indicated populations.
- (F) Pathway analysis was performed using Enrichr and graphed based on enrichment score for significant GO biological processes (-Log₁₀ (adjusted p value)).